3D textural evidence for the formation of ultra-high tenor precious metal bearing sulfide microdroplets in offset reefs: an extreme example from the Platinova Reef, Skaergaard Intrusion, Greenland

David A. Holwell[a*], Stephen J. Barnes[b], Margaux Le Vaillant[b], Reid R. Keays[c], Louise A. Fisher[b] and Richard Prasser[a]

[a]Department of Geology, University of Leicester, University Road, Leicester, LE1 7RH, UK. dah29@le.ac.uk richardprasser@btinternet.com

[b]Mineral Resources Flagship, Commonwealth Scientific and Industrial Research Organization (CSIRO), Kensington, Perth, WA 6151, Australia Steve.Barnes@csiro.au Margaux.Levaillant@csiro.au Louise.Fisher@csiro.au

[c]School of Geosciences, Monash University, Victoria 3800, Australia. reid.keays@monash.edu

*Corresponding author:

Tel: +44 (0) 116 252 3804

Fax: +44 (0) 116 252 3918

Revised version submitted to: Lithos

Abstract

The Platinova Reef in the Skaergaard Intrusion, east Greenland, is an example of a type of layered-intrusion-hosted, precious metal-enriched, stratiform, disseminated sulfide deposits referred to as “offset reefs”. These typically show platinum-group element (PGE) enrichment immediately below a major increase in the abundance of Cu-rich sulfides, with a prominent peak in Au enrichment exactly at that transition between the PGE-rich and the sulphide-rich zones. The reasons for the relative sequence of offsets in metal peaks, and the occasionally very high metal tenors have been subject to great debate. Here we use an integrated approach of high-resolution X-ray computed tomography (HRXCT), SEM, synchrotron and desktop microbeam XRF mapping, and thin section petrography to comprehensively classify the textural relations of the precious metal-bearing sulfides of the Platinova Reef as an extreme end member example of an exceedingly high tenor offset deposit. Our results show that in the zones of PGE enrichment, precious metal minerals (PMM) are intimately associated with Cu sulfide globules, mostly located at, or close to, silicate and oxide boundaries. The textures are identical in zones enriched in Pd and Au, and thus we do not see any evidence for different processes forming the different zones. The PMM:Cu sulfide ratio in each globule varies significantly but overall the size of the globules increases from the Pd-rich, through the Au-rich, and into the Cu zone, with a significant corresponding decrease in PM tenor. As such, this records a progression of exceedingly high tenor, microdroplets of sulfide, that progressively get larger up through the section, and decrease in tenor proportionally to their size. Cumulus droplets of Cu sulfide became enriched in metals, and were trapped *in situ* without significant transport from their point of nucleation. The transition to larger sulfides represents a change from sulfides nucleated and trapped *in situ*, to larger ones that liquated from a magma devoid of crystals and were able to grow and sink. This feature is common in all offset reef deposits, and is marked by the major enrichment in Au. Although the metal ratios of PGE to Au in the Pd- and Au-rich offset zones differ, the identical textures and comparable mineralogy show the physical mechanisms of concentration are the same in all zones indicating a similar physical method of concentration. The relative position of the Pd, Au and Cu peaks in the Platinova Reef is essentially the same as that in numerous other offset reefs, suggesting common overarching processes are responsible for the enrichment in metals, and relative offsets in peak metal concentrations in all such deposits. The most important of these processes are their relative $D_{sul/sil}$ values and the diffusivities of the metals, which determine the order of offsets and the high tenors of the smallest sulfide droplets. The Platinova Reef therefore records the extreme enrichment via

equilibrium and diffusive partitioning into sulfide liquid microdroplets very close to their point of nucleation.

Keywords:
Skaergaard, platinum-group elements, gold, microtomography, sulfide saturation,

1. Introduction

The Skaergaard Intrusion, east Greenland, is host to the Platinova Reef, a magmatic Cu-PGE-Au sulfide deposit that belongs to a relatively rare subclass of magmatic sulfide deposits. These deposits occur as stratiform layers in the upper parts of their host intrusion (e.g. Maier 2005) and are referred to as “offset reefs” (Godel, 2015). Other examples include the Ferguson Reef of the Munni Munni Complex (Barnes et al., 1992; Barnes, 1993; Barnes and Hoatson, 1994), the Main Sulfide Zone of the Great Dyke of Zimbabwe (Wilson and Tredoux, 1990), and the PGE-enriched layers of the Sonju Lake intrusion (Li et al., 2008), the Rincon del Tigre complex (Prendergast, 2000) and the Stella Intrusion, South Africa (Maier et al., 2003). These all display the essential characteristics of metal offsets within the mineralised interval, such as a distinct zonation with a Pt+Pd-rich peak(s) at the base, followed by a Au peak above this, and finally a Cu peak above that. The Cu peak corresponds to an abrupt increase in bulk sulfide content (Andersen et al., 1998; Prendergast, 2000; Nielsen et al., 2005; Holwell and Keays, 2014; Holwell et al., 2015). This sequence typically occupies a stratigraphic thickness ranging from a few metres to tens of metres. The sequence of metal concentration peaks is attributed in all of the studies cite above to the relative order of magnitude of sulfide liqud/silicate liquid partition coefficients for the elements in question, i.e. D_{Pd} =~D_{Pt}>> D_{Au} >D_{Cu}.

Characteristically, the mineralisation of the Platinova Reef consists largely of Pd(+Pt) and Au alloys intimately associated with sulfide globules composed of bornite and digenite/chalcocite with no significant Ni or Fe sulfides (e.g. Andersen et al., 1998; Nielsen et al., 2005; Nielsen et al. 2015; Holwell et al., in press). This mineralization is largely thought to have formed from the accumulation of very small droplets of Cu-rich magmatic sulfide liquids. These contain the highest recorded tenors of Pd (~10,000 ppm), Au (~15,000 ppm) and Se (<1200 ppm), and the lowest S/Se ratios (190-800) of any known magmatic sulfides (Holwell and Keays, 2014; Holwell et al., 2015). This factor alone makes the Platinova Reef an extremely important example, and possible end-member, of a magmatic system wherein certain processes have led to the formation of ultra-high tenor sulfides. In addition to the extreme tenors, the textures of the sulfides offer the opportunity to investigate extreme processes of metal enrichment in magmatic sulfides. Further to this, the extremely small size of the sulfides and their apparent trapping in situ presents both an opportunity to study sulfide microdroplets close to the point of nucleation; but also to investigate a problem when attempting to apply conventional mechanisms of metal concentration by sulfide-silicate interaction (the R factor; e.g. Campbell and Naldrett, 1979). The extreme tenors require mechanisms whereby tiny droplets can effectively extract Pd and Au

from magma volumes of the order of hundreds of thousands to millions of times their own volume to satisfy simple mass balance criteria, regardless of the precise mechanism.

Whilst the relationship to the onset of sulfide saturation may be clear, the processes responsible for some of the particularities of these reefs, including the metal offsets, the mineralogy, and the sulfide metal tenors are less clear and currently subject to a range of interpretations. Essentially, most of these processes are orthomagmatic, although the importance of late- and post magmatic fluids on the mobility and distribution of precious metals, and the possibility of S-loss through syn-magmatic dissolution or post-magmatic alteration remain subject to debate (Bird et al., 1991; Andersen et al., 1998; Prendergast, 2000; Maier et al., 2003; Nielsen et al., 2005; 2015; Wohlgemuth-Ueberwasser et al., 2013; Godel et al., 2014; Rudashevsky et al., 2014; 2015; Holwell and Keays, 2014; Keays and Tegner, 2015).

Whilst there have been a number of recent studies on the textures of the silicate and oxide phases in the Skaergaard Intrusion (e.g. Holness et al., 2007; 2011; Namur et al. 2014; Godel et al., 2014), this paper specifically focuses on the textures of the sulfides, precious metal minerals, and their relationship to each other and to the host gabbro cumulate minerals within the Platinova Reef. This study builds on previous work by Godel et al (2014) in having a larger number of samples, from a drill hole located closer to the side-wall of the intrusion and putting a greater emphasis on the gold-rich layer. We use an integrated approach of high-resolution X-ray computed tomography (HRXCT), SEM, synchrotron and desktop microbeam XRF mapping and thin section petrography to comprehensively classify the textural relations of the precious metal-bearing sulfides of the Platinova Reef. In particular, we focus on the three dimensional textures of the sulfides, precious metal minerals, and their relationship to each other. The combination of these techniques allows us to draw meaningful conclusions about the spatial distribution and relative compositional variation of composite precious metal – sulfide aggregates within an offset reef deposit.

2. Mechanisms of extreme precious metal enrichment in magmatic sulfide liquids

The processes involved in generating PGE-rich magmatic sulfide deposits are well established and summarised by Naldrett (2011) and references therein. Once a mafic/ultramafic magma has become saturated in sulfide, the enrichment of the sulfide in chalcophile elements such asPGE is determined by: (1) the initial concentration of the metals in the magma, which is in part a function of the degree of partial melting at the mantle source; (2) the ability for the sulfide to

interact with, and thus sequester chalcophile elements from large volumes of mafic magma; and (3) the relative partitioning of each element into sulfide liquid ($D_{sul/sil}$), which varies from several hundred for Ni and Cu, through to tens or hundreds of thousands for some of the PGE (Mungall and Brenan, 2014). All these factors can all be related through the equation of Campbell and Naldrett (1979)

$$Y_i = [D_i * Y_{oi} * (R + 1)]/(R + D_i) \quad (1)$$

where Y_i is the concentration of metal in the sulfide, D_i is the distribution coefficient between sulfide liquid and silicate magma of the metal, Y_{oi} is the original concentration of the metal in the magma, and R is the ratio between silicate magma and sulfide liquid. Attainment of high metal tenors requires equilibration of the sulfide with large amounts of silicate magma, i.e. high values of R. Mungall (2002) showed that this equilibration is limited by relative rates of magmatic diffusion of the various chemical components of the sulfide melt, including S, and that very high tenor and very high effective R factors are the expected result when very small, approaching infinitesimal, amounts of sulfide first nucleate from a magma.).

The Pd and Au tenors of the Platinova Reef are very high, in the region of 10^4 ppm (Holwell and Keays, 2014) (The average Pd tenor of the main Pd peak in the drill hole (PRL-08-35A) from which samples were taken, is 7780 ppm. Assuming that the Pd content of the magma at the time of formation of the Platinova Reef was 43 ppb, as estimated by Keays and Tegner (2015), and that D_{Pd} is 540,000 (Mungall and Brenan, 2014), equation (1) can be used to derive an R-factor value of $2.7 * 10^5$. A single stage batch equilibration model would require a highly unusual mechanism to attain such a very high R-factor. .

Several processes can explain very high precious metal tenors in sulfides in addition to the simple batch equilibrium model to which the R factor model applies. Syn-magmatic processes include pre-formation of platinum-group minerals (PGM) prior to collection by sulfide liquids or chromite crystals (Tredoux et al., 1995; Ohnenstter et al., 1999; Ballhaus and Sylvester, 2000; Helmy et al., 2013). Direct precipitation of PGM from silicate melt caused by the saturation in certain phases has also been proposed as a possible mechanism for producing PGE-enriched layers with little to no associated sulfide (e.g. Maier et al., 2015; Barnes et al., 2016). Another syn-magmatic process was proposed by Mungall (2002), who showed that the concentration of any element in a sulfide liquid is a function not only of how chalcophile that element is (the equilibrium metal partitioning coefficient, $D_{sul/sil}$) but also the relative diffusivities of the most chalcophile elements. He showed that that the interplay of fractional sulfide segregation with

diffusion-controlled disequilibrium could produce a remarkably faithful duplication of offset metal profiles, using the example of the PGE-enriched offset sulfide reef in the Munni Munni intrusion. At the point of nucleation, sulfide droplets could attain exceedingly high metal tenors however, under conditions where R>>D, the maximum metal tenor of any increment of sulfide can never exceed the limit determined by the D value. Hence, for this mechanism to apply in the Platinova Reef, effective D values must still have been extreme.

A number of syn- and post-magmatic processes may occur to modify sulfide droplets once they have formed. This includes partial dissolution upgrading, whereby sulfides partially re-dissolve back into sulfide-undersaturated magma, thus greatly increasing R factors and hence creating sulfides with very high tenors (Kerr and Leitch, 2005). Godel et al (2014) found textural evidence in the Platinova Reef consistent with this model. Wohlgemuth-Ueberwasser et al. (2012) proposed selective postcumulus oxidation of Fe sulfides giving rise to a reduction in sulfide volume through incongruent dissolution and a consequent increase in Cu content. Finally, post-magmatic hydrothermal alteration of sulfides has the potential to remove sulfide preferentially over precious metals, which would also increase the metal tenor of the sulfides.

Nielsen et al. (2015) proposed a complex model for the Platinova Reef specifically, in which high precious metal (PM) tenors are the result of pre-concentration of PM in a segregated and internally differentiated mush layer at the base of intrusion, followed by partial redissolution in a migrating intercumulus Fe-rich immiscible melt, and upward migration of Au due to interaction with a late-exsolving free volatile phase. This model predicts that the paragenetic association of Au with sulfides in the Au-rich component of the Platinova package should be distinctly different from the equivalent Pd-sulfide association.

3. The Platinova Reef

The Skaergaard Intrusion, Kangerlussuag region, east Greenland (Fig. 1A) was emplaced at 56.02 Ma (Wotzlaw et al., 2012) during widespread Paleogene magmatic activity associated with the opening of the north Atlantic Ocean and passage of Greenland over the proto-Iceland plume (e.g. Brooks and Nielsen, 1982; Tegner et al., 1998; Saunders et al., 1997; Momme et al., 2002). One of the key characteristics of the Skaergaard Intrusion is that it crystallised under closed system conditions from a single, homogeneous body of magma and has thus become the type example for studies of magmatic layering and differentiation (e.g. Wager and Brown,

1968; McBirney, 1989; Irvine et al., 1998; Holness et al., 2007; Tegner et al., 2009; Thy et al., 2009; McKenzie, 2011; Holness et al., 2011, Keays and Tegner, 2015; Nielsen et al., 2015).

The Skaergaard Intrusion consists of three main units, *viz*: the Layered Series, formed through crystallisation from the floor up; the Upper Border Series, a mirrored sequence of the Layered Series that crystallised from the roof down; and the Marginal Border Series that crystallised inwards from the outer walls of the intrusion. The Layered Series is split into zones according to cumulus mineralogy and consists of the Hidden, Lower, Middle and Upper Zones (Fig. 1B). The Platinova Reef is located in the uppermost part of the Middle Zone in the Triple Group: a 100m-thick unit of modally layered plagioclase-clinopyroxene-Fe/Ti-oxide gabbros with three prominent leucocratic layers (Fig. 1C) visible in the field that give the unit its name.

Sulfide mineralisation is present as tiny sub-millimetre grains of bornite-digenite/chalcocite with associated precious metal-bearing minerals that are dominantly Pd-Pt-Au-Cu-Fe-alloys (Bird et al., 1991; Andersen et al., 1998; Rudashevsky et al., 2004; Cabri et al., 2005; Nielsen et al., 2005; 2015; McDonald et al., 2009; Godel et al., 2014; Rudashevsky et al., 2014; 2015; Holwell et al., in press). Precious metals are enriched in a series of stratiform layers, The lowermost precious metal layer is the main Pd-bearing layer (designated Pd5 by Nielsen et al., 2015), and is present across the entire intrusion. Further layers are then present above this, which reduce in their lateral extent upwards, and appear to have Au-rich edges (Fig. 1C). This means that in any one location there is a lower Pd rich zone and a Au-rich layer above it, up to 40 m above it in the central parts of the intrusion, and only a few metres above it at the margins. Previous authors have made an analogy to a stack of gold-rimmed plates; Pd rich in the centre and Au rich at the edge, becoming smaller up-section such that the Au-rich edge of the upper plate overlies the Pd-rich interior of a lower one (Andersen et al., 1998; Nielsen et al., 2015). The top of the stack of precious metal-enriched zones is marked by a sharp increase in modal Cu-rich sulfide content within a continuous layer extending across the entire complex. The principal Au peak occurs exactly at the base of this Cu-rich layer, exactly at the sharp transition to higher volumes of sulfide, where Cu contents increase from a few tens to a few hundreds of ppm (Holwell and Keays 2014).

Here we use the simplified zonation for the mineralised zone based on the relative metal enrichments (Holwell and Keays, 2014; Fig 1C): the Subzone is stratiform and concordant and present beneath the lowermost leucocratic layer of the Triple Group, L0, where PGE

concentrations start to increase upwards; the Pd zone (Pd >1 ppm; Pd5 of Nielsen et al., 2005; 2015) is stratiform and concordant, and located within the L0 unit; the Intermediate zone which is a weakly mineralised (Pd 0.1-1 ppm) zone with multiple small Pd peaks is of variable thickness and is bounded at its base by the stratiform Pd zone; a thin Au zone (Au >1 ppm; UAuM of Nielsen et al., 2015) which is present within a few metres of the Pd zone at the intrusion margins, and up to 40 m above it in the centre and is thought to be discordant (Nielsen et al., 2015); and the Cu zone, where Cu contents are consistently >200 ppm and precious metals contents are <1 ppm. This constitutes all rocks in the Triple Group above the Au zone. The mineralization below the Cu zone consists of microdroplets of sulfide (typically <100 μm) with Pd and Au tenors of 10^{3-4} ppm, Pd/Au ratios >1, S/Se ratios 500-800 and low Cu/Pd ratios, whereas the sulfides in the Cu zone are larger (100-1000 μm), have considerably lower tenors (10^{1-2} ppm Pd), Pd/Au ratios of <1, S/Se ratios as low as 190 and high Cu/Pd ratios (Holwell and Keays, 2014; Holwell et al., 2015). However, the sulfide mineralogy in all zones is consistent, being comprised of bornite-digenite/chalcocite exsolution intergrowths (Nielsen et al., 2015).

Previous studies have attributed some of the characteristic features of the mineralisation to (1) fractionation of sulfide liquids (Andersen et al., 1998); (2) the presence of immiscible Au-rich melts and sulfide liquids (Bird et al., 1991); (3) filter pressing of sulfide liquid (Andersen et al., 1998); (4) Rayleigh fractionation processes (Prendergast, 2000); (5) oxidation of sulfides (Wohlgemuth-Ueberwasser et al., 2013); (6) late stage redistribution of metals by a volatile phase with deposition at redox boundaries (Andersen, 2006; Rudashevsky et al., 2015; Nielsen et al., 2015); (7) major post-magmatic S loss by fluids (Andersen, 2006); (8) syn-magmatic dissolution of sulfide droplets (Nielsen, 2013; Godel et al., 2014; Holwell and Keays, 2014; Nielsen et al., 2015); and (9) redox fluctuations linked to magnetite formation converting sulfate to sulfide (Keays and Tegner, 2015).

4. Sampling and methods

Fourteen samples were taken from the diamond drillhole PRL08-35A, drilled by Platina Resources Limited in 2008 (Fig. 1A). The core intersects the Subzone, Pd zone, Intermediate zone, Au zone and lower parts of the Cu zone without interruption from dykes or offsets due to faults (Fig. 1C). Samples were selected to cover a range of mineralised zones including two from the subzone (at 335 and 332 m), four from the Pd zone (328, 327, 326, 325 m), one from the thin Intermediate zone (322 m), five from the Au zone (at 20 cm intervals from 319.0 m) and two from the Cu zone (306 and 297 m). Bulk rock geochemistry on 20 cm intervals through the

entire section was provided by Platina Resources, and was generated at Genalysis Laboratory Services, Western Australia using Pb collection fire assay followed by Inductively Coupled Plasma-Mass Spectrometry for the precious metals and X-ray Fluorescence on fusion disks for TiO_2 and V.

Sulfide and precious metal mineralogy and textures were observed and documented in reflected light and by Scanning Electron Microscope (SEM) at the University of Leicester using a Hitachi S-3600N SEM, coupled with an Oxford Instruments INCA 350 energy dispersive X-ray analysis system.

High resolution X-ray Computed Tomography (HRXCT) 3D analysis was performed on three representative samples: 327 (Pd zone), 319.2 (Au zone) and 306 (Cu zone) to observe the textural relationships and the distribution of sulfides and precious metal minerals within the samples. Samples were 3 mm cores, of 30 mm length. They were analysed using the XRADIA XRM High-resolution 3D X-Ray microscope system at the Australian Resources Research Centre (ARRC, Perth, Australia). The analytical technique and data processing protocol is described in detail in Godel (2013). Parameters used for the analysis were a voltage of 110 kV, a power of 10 W and a pixel size between 1.523 and 1.533 µm. A total of 2000 2D projections were collected per 360° rotation of the sample, which were used to reconstruct the 3D volumes using AvizoFire® (Visualization Sciences Group) software coupled with dedicated CSIRO-developed workflows and software designed for ore materials.

X-ray fluorescence (XRF) microscopy was performed on the XFM beamline at the Australian Synchrotron (Paterson et al. 2011) using the Kirkpatrick Baez mirror microprobe end-station. Further details of the analytical procedure can be found in the Supplementary Material.

Thin-section scale mapping was carried out on conventional polished thin sections using a Bruker M4 Tornado™ desktop scanning x-ray fluorescence spectrometer (µ-XRF), with a 40 micron polychromatic beam generated from a Rh tube operating at 50 kV and 500 nA, and signal collection using an Xflash™ silicon drift detector. Maps were scanned at 40 micron resolution using a dwell time of 10 ms per pixel, and processed initially using Bruker's proprietary Esprit™ software. Phase maps were generated using a clustering algorithm within CSIRO proprietary Chimage™ software (Wilson and MacRae, 2005).

5. Petrology of the mineralised zones

The Triple Group is made up of modally layered Ti-rich gabbros containing lath-like plagioclases, with clinopyroxene, orthopyroxene after inverted pigeonite, ilmenite, and titanomagnetite (Andersen et al., 1998). The reactive symplectites and olivine reaction rims observed by Holness et al. (2011) that are most common in the central parts of the intrusion, interpreted by them to be evidence for immiscible Fe- and Si-rich melts, are totally absent in our samples from closer to the intrusion margin. Here we show further petrological information gained from desktop XRF mapping to illustrate the distribution of sulfide blebs, interstitial melt pockets and the modal petrology of the rocks.

5.1. Desktop XRF mapping of sulfide distribution

Desktop “Tornado” maps were collected over eight thin sections, and converted to phase maps. Results from three selected samples, one each from the Cu, Au and Pd zones, are shown in Figures 2 and 3. A distinct fabric caused by the alignment of plagioclase is evident in all three samples and is parallel to layering in the intrusion (Fig. 2A). Plagioclase is coarser grained than the oxide and pyroxene phases, which together form clustered interconnecting networks, particularly evident in Au zone sample 319.4 (Fig. 2B). Both ilmenite and titano-magnetite are clearly cumulus phases, forming chains of equant, anhedral grains, corresponding to the P1 paragenesis of Nielsen et al (2015).

The distribution of sulfide minerals (a complex exsolution texture of bornite and digenite/chalcocite in all zones) in relation to the cumulus silicate-oxide framework can be ascertained from the four-element maps of Cu, K, P and Fe distribution (Fig. 3). These maps show the spatial distribution of sulfides (red), K-feldspar (green) and apatite (blue) in relation to plagioclase, pyroxenes and oxides, which have different shades of grey determined by their respective Fe contents. The proportion of sulfide aggregates that occur at different types of cumulus grain boundaries are shown in the associated pie charts in Figure 3, which refer to all eight sections imaged. Sulphide grains appear bigger than they are in Tornado images because of the greater penetration of the Cu X-rays through the silicate matrix. The Pd and Au zone have very similar sulfide associations, with around 75% of the sulphides occurring at the boundaries of pyroxene grains (either with other pyroxenes, or with plagioclase), and a quarter associated with oxides. The slightly higher proportion of plagioclase-associated sulfides in the Pd zone compared with the Cu zone (Fig. 3D,F) is reflective of the higher modal proportion of plagioclase (Fig. 3DC,E), with the Pd zone located in the L0 layer, which has 50% modal plagioclase

(Andersen et al. 1998), and the Au zone in our samples located within a more melanocratic unit. This 2D spatial analysis indicates that the great majority of sulfide blebs are located at or within a few microns of grain boundaries of cumulus silicates and oxides, and in most cases are randomly located along different boundary types in rough proportion to the modal abundance of the phases.

The Cu zone samples (one of which was taken from the plagioclase-rich L1 layer at 306 m) show a somewhat greater proportion of sulfides present at oxide grain boundaries, with 49% of sulfide aggregates attached to Fe-Ti oxides in the two samples studied (from 306 and 297 m). Even taking into account the modal mineralogy, there is a slightly larger preference for sulfides to be associated with oxide grain boundaries in this zone than there is in the Au and Pd zones.

The distributions of K and P are significant in recording the final disposition of trapped intercumulus components. It might be expected that K-feldspar (imaged by the K abundance in Fig. 3) and apatite (imaged by P) would show a strong spatial association, as both are postcumulus phases that would be expected to have crystallised from the last segregated dregs of the intercumulus liquid. However, this is not observed; except for one small pocket in section 306 (Fig. 3A) these components are randomly distributed, with K-feldspar showing a strong preference for plagioclase grain margins (presumably reflecting reaction of plagioclase with trapped liquid), including around the edges of poly-grain aggregates, which gives the false appearance in Figure 3 of there being inclusions of K-feldspar in plagioclase.

5.2. Sulfide-silicate inclusions in oxides

An interesting feature observed in several of our samples, from all zones, is the presence of rounded sulfide-silicate inclusions within ilmenite (Fig. 4). This apparently shows the entrapment of droplets of silicate magma with sulfide droplets. The sulfides and their associated PMM are identical to those found elsewhere (Fig 4). The silicates are largely hydrous assemblages of biotite, quartz and amphibole, similar to the population of entirely hydrous silicates identified by Godel et al. (2014). Figure 4C shows a trail of very small silicate inclusions identical to some of those imaged in 3D by Godel et al. (2014).

6. Bulk rock geochemical profiles

Figure 5 and Table 1 shows detailed metal profiles through drill hole PRL08-35A, including the well-established Pd, Au and Cu patterns defining the various mineralisation zones (Fig. 5A), and

thin section photographs to illustrate the modal mineralogy. Previous studies have used samples on a 1 m spacing (e.g. Holwell and Keays, 2014) or 25 cm spacing (Nielsen et al., 2015). We show, for the first time, a profile through the Platinova Reef using continuous 20cm samples to show the geochemical profiles on a resolution not previously possible. This shows the Au zone to be entirely contained within a single metre intersection, with a very sharp peak on this scale, showing the highest grade to be within a few tens of centimetres.

A number of studies invoke magnetite crystallisation as an important trigger for sulfide saturation in offset deposits (e.g. Prendergast, 2000; Andersen, 2006; Maier et al., 2003; Keays and Tegner, 2015). Holwell and Keays (2014) also suggest this as a possible mechanism in Skaergaard, by demonstrating a general, but loose, correlation between Pd and V as proxies for sulfide and magnetite, respectively, on a 1 m sample scale. Using the higher resolution dataset here, it can be seen that there is a distinct peak in V and TiO_2 at the base of the Pd zone (Fig. 5B). The increase in Pd at the base of the Pd zone matches very closely the point where there is a particularly oxide-rich layer (~9 wt% TiO_2 and >1000 ppm V), illustrated by the differences in thin sections from 328m and 325m (Fig. 5C). Note how the proportion of plagioclase is similar in these two samples, with the major difference being the pyroxene:oxide ratio, with the sample from 325 m containing only a few modal percent oxide corresponding to the TiO_2 and V minima in Figure 5B. The relationship of a consistent, thin (< 1m) peak in TiO_2 and V located immediately below the main Pd peak has been tested in other drill holes and proven to be a consistent feature of the Platinova Reef (Prasser et al., 2015).

7. Precious metal mineralogy

The mineralogy of the PGE and Au minerals of the Platinova Reef has been described in detail elsewhere (e.g. Nielsen et al., 2005; Cabri et al., 2005; Nielsen et al., 2015 and references therein) and so here we only report the minerals identified in the samples we have studied that are thus directly relevant to our textural observations on the same samples. Table 2 lists 100 precious metal minerals (PMM) identified within our samples from the various zones within the Platinova Reef, and Figure 6A shows the varying proportions of different PMM type in each of the samples.

Our samples are taken from close to the margin of the intrusion, where the PMM mineralogy is known to include a wider range of minerals than the more Pd-Au-Cu alloy dominant central portion (Nielsen et al. 2015). In our samples, the subzone contains a varied assemblage of

zvyagintsevite (Pd_3Pb), Pd tellurides, arsenides and the sulfide vysotskite (PdS). The apparently high proportion of PGE sulfides (Fig 6A) is due to a single large grain skewing the percentage by area. The Pd zone is dominated by the Pd-Cu alloy Skaergaardite (PdCu); with some zvyagintsevite, sulfides including vysotskite and braggite ((Pt,Pd)S), and atokite (Pd_3Sn). Figure 6B shows an example of an altered sulfide bleb, with secondary silicates cutting across both sulfide and zvyagintsevite, with the latter apparently present prior to alteration. The Au zone is dominated by Au-(Pd)Cu alloys and electrum, with some Pd arsenides such as vincentite (Pd_3As). The majority of the Au-Cu alloys in our samples are Au_3Cu, rather than tetra-auricupride (AuCu), which is reported to be the most common Au mineral in other studies (e.g. Nielsen et al., 2005). Nielsen et al. (2015) also note Au_3Cu increases in abundance close to the intrusion margins. Texturally, the Au_3Cu is located within the margins of the sulfide blebs in the same way most other PMM do (Fig 6C). The base of the Cu zone includes some PMM, including electrum, tetra-auricupride and some Pd arsenides such as palarstanide ($Pd_5(As,Sn)_2$).

8. Textural associations of the sulfides and precious metal minerals

The 2D and 3D textural relationships of the sulfides have been analysed by synchrotron XFM and High Resolution X-ray CT techniques, respectively.

8.1. Synchrotron data

Synchrotron XFM mapping located 195 individual precious metal grains associated with about 67 Cu-Fe sulfide blebs (or their alteration products) in seven 100 µm-thick polished sections: three from the Pd zone and four from the Au zone. The high energy of the x-ray beam used in this technique results in complete penetration of the 100 micron thick section, such that the maps record the position of PM and Cu-rich grains anywhere within the section, in contrast to SEM and optical images that only show grains on the surface. Examples of the cm^2 and mm^2 scale detailed maps of one sample each from the Pd and Au zone are given in Figures 7 and 8, respectively. Results are tabulated in Table 3, showing details of the textural association, location in relation to cumulus mineral species and degree of alteration of the associated sulfide droplet for all identified PM grains. The relative proportion of PMM, the degree of alteration of the blebs, and the textural association between PMM and the immediately associated phase in Table 3, are plotted as pie charts in Figure 9.

The major point to emerge from the high resolution synchrotron XFM results is that the textural relationships of the sulfide blebs (Fig. 9A,B) and the relationships between PMM grains and sulfide blebs (Fig. 9C,D) are similar between the Au and Pd zones. The sulfides in both zones have similar and roughly equal proportions that are included in primary minerals, at oxide grain boundaries, and at silicate grain boundaries (Fig. 9. A,B). Almost all of the sulfide blebs that were imaged showed a close spatial association with PMM grains. Between 70 and 80% of all PMM were observed to be in direct contact with sulfide (Figure 9C,D). In most cases PMM grains were observed to be at the margin of a sulfide bleb, or lying a few microns outside; the latter association tends to apply to the more ragged blebs (e.g. Fig. 7B, 8B), implying that some sulfide has been lost in this setting to alteration, but that the PMM remained . Typically multiple PMM grains were found within each sulfide bleb, although one or two larger ones usually dominate (e.g. Fig. 7H, 8). The synchrotron XFM maps confirm the strong association of these composite grains with the contacts between cumulus minerals, most commonly between pyroxene grains and either other pyroxene grains or oxides (e.g. Fig. 7F, 8A,F,G). Distinct "eyeballs" with a single PMM associated with a subrounded bleb were most commonly observed within Au zone samples (e.g. Fig. 8A) but are not exclusive to this zone. The lack of any systematic correlation between textural associations and hydrothermal alteration implies that alteration was a purely superimposed effect that had no significant impact on the distribution of the PMM.

8.2. High resolution 3D X-ray microtomography

High resolution x-ray microtomographic images were collected on 3 samples, one each from the Pd, Au and Cu zones, and representative images are shown in Figures 10 and 11.

8.2.1. Sulfide-silicate-oxide relationships

Figure 10 shows a number of slices through the 3D reconstructions of samples from the Pd zone (Fig. 10A-C), the Au zone (Fig. 10D-F) and the Cu zone (Fig. 10G-I). Movies showing sequential time slice animations through each of the samples are included in the Electronic Appendix (Figs. A1-3). In agreement with the 2D techniques, most sulfides are located at, or near grain boundaries. Sulfide droplets in the Pd zone are the smallest (< 100 μm) and are almost always associated with at least one PMM. The sulfides are variably altered as seen by a continuum from very fresh, rounded sulfides, through slightly altered sulfides (Fig 10A) to patches of almost totally replaced sulfides, seen as small patches of fine grained sulfides overprinted by secondary silicates (Fig. 10B). Sulfide droplets within oxide grains have not

472 undergone as much alteration, and are usually present as rounded droplets of sulfide; however
473 we have observed a number of rounded inclusions within oxides that are made up of sulfide,
474 PMM and silicates, and appear to represent trapped droplets of sulfide and silicate (Fig. 10C).
475 The sequential slice movies (Electronic Appendix Figs. A1-3) prove without doubt that these are
476 rounded droplets entirely enclosed by oxide and do not represent fracture fills or fortuitously
477 sectioned tubular embayments.
478
479 The Au zone displays almost identical textures, with sulfides present associated with pyroxenes
480 (Fig. 10D) and oxides in general, with a continuum of textures from rounded and unaltered (Fig.
481 10D), to examples where the sulfide has been variably altered to secondary silicates (Fig. 10E).
482 There is a slight increase in the size of some of the sulfide blebs compared with the Pd zone, as
483 seen in Figure 10E, with some blebs up to 200 μm in diameter. In addition to examples of
484 rounded inclusions of sulfide and silicate in oxides, there are also examples of rounded silicate
485 inclusions without any sulfide (Fig. 10F; 4C), as seen by Godel et al. (2014).
486
487 The sample from the base of the Cu zone shows a marked increase in the size of the sulfide
488 droplets (typically >200 μm), with mostly rounded blebs present associated with pyroxenes and
489 oxides (Fig. 10G), though many show similar alteration around their margins to those in the
490 other zones (Fig. 10H). This alteration is less pronounced due to the original larger size of the
491 grains, and thus the alteration around the margins is proportionately less pervasive than it is for
492 a much smaller grain. Some small PMM are observed (Fig. 10H). Sulfides are present within
493 oxides as rounded droplets with silicate, as they are in the other zones. However, unlike in the
494 other zones, sulfides display a tendency to preferentially attach themselves to the surfaces of
495 oxides grains such as ilmenite (Fig. 10I; A3).
496
497 8.2.2. Sulfide-precious metal mineral relationships
498 Figure 11 illustrates a number of typical variants of sulfides in the Cu (Fig. 11A-C), Au (Fig. 11D-
499 F) and Pd zones (Fig. 11G-I): (1) “eyeballs”, where single PMM grains lie at the edges of much
500 larger Cu-Fe sulfide droplets (Fig. 11A,B,G), which form a continuum with; (2) smaller blebs with
501 spherical to irregular morphologies containing a high proportion of PMM to Cu-Fe sulfide (Fig.
502 11D,G), or in some cases being almost entirely composed of PM with very little sulfide (Fig.
503 11C,I); and (3) irregular sulfide aggregates with multiple PMs of variable size (Fig. 11E,H). In
504 some cases the irregular multi-PM blebs appear to be the result of alteration of more regular
505 magmatic blebs, but this is not universal.

The 3D data allow firm conclusions to be drawn about textural associations without the usual stereological ambiguities and biases arising from 2D sections. Statistics are compared in Figure 12 on observations on 137 grains from the 3D-scanned samples from all three zones. We compared the distribution of sulfide-PMM blebs after dividing them into three categories - high Cu/PMM blebs with a volume ratio of PM/sulphides between 10^{-5} and 0.01; small PMM-dominated (low Cu/PMM) blebs with a volume ratio of PM/sulphides between 0.01 and 1, and isolated PMs with little or no associated sulfides (Fig. 12) with a volume ratio of PM/sulphides between 1 and 1.10^{5}. All three types are equally likely to be sited at any of the various grain boundary types (allowing for the fact that some of these types, such as pyroxenes, are more common than others; Fig 12B,D,F). The proportion of larger sulfide blebs increases from the Pd, through Au to the Cu zone, with a concurrent reduction in PMM with little to no sulfide (Fig. 12A,C,E), and the Au zone represents a transition between small, PMM dominant blebs in the Pd zone, and the large sulfide blebs of the Cu zone.

The size and ratios of PMM and sulfide grains is presented in Figure 13, as equivalent sphere diameter (ESD), determined by the 3D HRXCT analysis. The size of PMM within sulfide droplets is generally similar in the Au and Pd zones (Fig. 13B,C), and smaller in the PMM-poor Cu zone (Fig. 13A). Figure 13D and E shows the ratio of PMM to sulfide sizes as a ratio of their respective ESD and volumes. This clearly shows that there is a systematic progression of proportionally increasing sulfide up through the three zones. From Figure 13B and C, there is no difference in the size of the PMM in the Pd and Au zones, thus the effect shown in Figures 13D and E is entirely due to increased sulfide volume in the Au zone, in comparison to the Pd zone. Figure 13F confirms this and shows that volumetrically, there is more sulfide in Au zone than the Pd zone.

9. Discussion

As noted in the introduction, the characteristic, sequential offsets in PGE, Au and Cu peaks are not unique to the Skaergaard intrusion. This pattern is exactly the same as is observed in other offset PGE Reefs: e.g. Stella, Rincon del Tigre, Sonju Lake, Munni Munni, and the Great Dyke (Table 1 of Maier et al., 2003, Figure 4 of Prendergast, 2000, Figure 6 of Li et al., 2007; Figure 6 of Barnes, 1993; Figure 12 of Wilson and Tredoux, 1990, respectively). This similarity exists notwithstanding substantial difference in detail, such as the multiple sub-layers within the Platinova package (Fig. 1C), and a wide variability in thickness (a few metres at Munni Munni,

several tens of metres at Rincon del Tigre), and a magnetite association in some cases (Stella and Rincon del Tigre) but not others (Munni Munni and the Great Dyke). On this basis, it is hard to believe that the Platinova system represents a fundamentally different set of processes than these other examples. Therefore, whilst we discuss our textural observations specifically for the Platinova Reef, we extend the inference that some of the fundamental physical and geochemical processes are ones that must apply to similar magmatic systems anywhere.

9.1. Textural relationships between sulfides and host phases: sulfide droplet formation

9.1.1. The precious metal enriched zones

Texturally, the sulfide blebs (with associated PMM) in the Au and Pd zones display no significant differences in terms of their association with host cumulus phases and importantly, there is no spatial association between sulfides with what are interpreted to be late intercumulus phases (Fig. 3). There is an increase in the number of larger sulfide blebs in the Au zone, compared with the Pd zone (Fig. 12,13), in line with Au enrichment occurring as sulfide volume starts to increase; common to all offset reefs. The presence of a very small modal proportion of intercumulus phases (Fig. 3) is interpreted to mirror the presence of only very small volumes of trapped interstitial melt; consistent with results from Tegner et al. (2009) who calculated the amount of trapped melt within the Triple Group to be around 2-5 %. These observations together imply that sulfides were not derived from a late-crystallising intercumulus liquid, but instead are a genuinely cumulus phase; a conclusion also favoured by Godel et al. (2014). Trapping of these very small cumulus droplets in the Pd zone almost certainly happened very close to where they initially became incorporated into the cumulus crystal mush, given that the size of the droplets is likely to preclude the possibility of any significant gravity-driven percolation through the intercumulus porosity (Chung and Mungall, 2009; Holwell and Keays, 2014; Nielsen et al., 2015).

This raises the question of how the tiny, extremely PMM enriched sulfide droplets of the Pd and Au zones became incorporated into the cumulus pile. An argument has been in progress for many years on the relative roles in cumulate formation of mechanical accumulation of crystals nucleated elsewhere, relative to *in-situ* nucleation and growth of crystals in the location where they are now observed. For example, recent observations on the Bushveld Complex and Rum Intrusion (Latypov et al. 2013; 2015) provide strong support to the hypothesis that PGE Reefs, containing extremely PGE enriched sulfide droplets, can form by an *in situ* nucleation and growth mechanism. In such models, high R factors are attained as a result of reaction between

sulfide droplets that are nucleated within a static mush layer at the interface between the magma and the cumulus pile, and magma convecting over that interface. This process is referred to as *in situ* reef formation by Latypov et al. (2013), and we consider it here as a possible explanation for our observations.

9.1.2. The precious metal-poor Cu zone and the transition in sulfide volume

The larger sulfides in the Cu zone show a slight preference to be located at cumulus oxide grain boundaries (Figs. 3B; 10I, A3). The relationship of the sulfides with oxides in this zone may reflect mild preferential wetting properties of sulfides on the oxides (e.g. Brenan and Rose, 2002). Holwell and Keays (2014) suggested the sulfides in this zone had undergone some degree of gravitational settling from the overlying magma column, and thus the ability to grow. Again there is no spatial preference to intercumulus/late cumulus phases (Fig. 3E), and the sulfides of the Cu zone are interpreted as being a mechanically sedimented cumulus phase. The low PM content of the Cu zone reflects PM depletion in the main magma body as a result of extraction into the lower PM-rich layers of the Reef, in line with previously proposed models of PGE depletion by progressive fractional sulfide segregation in offset-type reefs (e.g. Barnes 1993).

We suggest that the stratigraphic transition to higher volumes of sulfide records the onset of chamber-wide sulfide saturation. The very small size of the sulfide droplets below the transition reflects *in situ* nucleation in the crystal mush at the floor. These droplets are trapped, as microdroplets, *without* coalescing or growing more than a few tens of microns. Droplets in the main part of the chamber have the ability to grow from the convecting magma and accumulate at the floor. The transition to higher volume, PM-poor Cu sulfides seen in all offset reef deposits thus marks the point where the first arrival of this wave of allochthonous (i.e. nucleated elsewhere) chamber-derived sulfides hits the floor. Thus, it reflects a transition from *in-situ* nucleatation to mechanical accumulation of sulfides. This would also imply a high R factor for the larger sulfides, but the low tenor indicates precious metals had been depleted before they formed. Depletion of the magma in high D value elements like the PGE could be explained by the mechanism of convecting magma interacting with a static mush layer as mentioned above (Latypov et al. 2013).

This transition also appears to coincide with the main Au peak, which in all such deposits coincides with an increase in the volume of sulfide, before the first Cu peak. Our size data

shows this transition in sulfide size accordingly (Fig. 13F), and thus Au enrichment occurs at precisely the point where sulfide volumes start to increase, but does so in a very thin zone. This is shown in Figure 5, with the very thin (< 1m) Au peak coinciding precisely with the increase in sulfide as traced by Cu.

9.2. Textural relationships between PMM and sulfides: precious metal enrichment

There is an extremely strong spatial association between PMM grains and Cu-rich sulfide blebs, which attests to the original collection of PGE and Au by immiscible Cu-Fe sulfide liquid throughout the Platinova Reef. Furthermore, the textural relationship of PMM (as Pd-Pt-Cu of Pd-Pb alloys in the case of the Pd zone, and Au-Cu alloys in the Au zone) with their associated sulfide droplets is essentially identical between the Pd and Au zones, implying a similar physical mode of accumulation in both zones, but with different resultant geochemical characters.

At the broadest scale, the relationship between sulfide volume and PM tenor is inverse (Fig. 13E), which would be expected if the growing droplets start at very high R factors and evolve to grow progressively and thus reduce the R factor. However, our work shows that there is a wide variability of more than two orders of magnitude in the proportions of Pd or Au minerals to Cu sulfide within individual sulfide blebs in the same few cubic mm, as determined by full 3D imaging (Figs. 13; A1-3; Table A1). Such apparent variation in PMM to sulfide ratio on a droplet-by-droplet scale can be seen in Figure 9 of Cabri et al. (2005) in 2D, though this could be a function of where each grain was sectioned. The confidence that the 3D information affords (Figs. A1-3; and Godel et al. 2014) means that we can state unequivocally that the variability is real, and not a function of the 2D sectioning effects that can restrict traditional mineralogical deportment studies. This means that whilst the metal tenors calculated by Holwell and Keays (2014) in the range 10^3 to 10^4 ppm Pd and Au are average tenors on a metre sample scale, each individual droplet, however, may have tenors ranging from a few ppm to tens of percent. Whilst in the altered sulfides, this can easily be explained by reduction in volume of the sulfide, this relationship holds true for the rounded, ‘eyeball’ types and rounded to irregular grains with high PMM contents (e.g. Fig. 11A,C,D,F,J).

This variability in PM tenor of the sulfide component at the individual bleb scale is not associated with particular textural microenvironments, with the exception of blebs enclosed within cumulus oxide phases in the Pd zone, which were shown by Godel et al. (2014) to have systematically lower tenors relative to those outside. These enclosed blebs were very rare in the

642 samples studied in this investigation, and we conclude that they make up a very small
643 contribution to the overall sulfide population. Here we assess three possible explanations for the
644 wide variability in individual metal tenor that can potentially be tested with the data we present
645 above, in the context of current knowledge of magmatic PM geochemistry.
646 1. Separate nucleation of PMM and sulfide droplets
647 2. Formation of extremely PM-enriched Cu-sulfide with subsequent modification
648 3. The effect of equilibrium and kinetic partitioning around growing sulfide droplets
649
650 9.2.1 Separate nucleation of PMM and sulfide droplets
651 In this model, Cu-rich sulfide liquid and PMMs grew independently from a Pd-Cu (or Au-Cu, Pd-
652 Pb, etc.) metal-saturated silicate magma and are physically associated by some process. Given
653 the very strong spatial association between them, if separate nucleation did happen, then the
654 two phases must have had an extremely strong affinity to each other after initial formation. The
655 generation of PMM directly from a magma has been suggested as a possible mechanism for
656 producing PGE-enriched horizons with little to no base metal sulfides, such as Pt phases in the
657 Monts de Cristal intrusion, Gabon (e.g. Maier et al., 2015; Barnes et al., 2016). This model,
658 initially proposed to explain extreme PGE enrichment in trace sulfides in the Munni Munni
659 intrusion (Barnes, 1993) may provide an explanation as to how the sulfide droplets became so
660 highly enriched in precious metals, if the PGE and Au were effectively pre-concentrated by
661 formation of metal alloys.
662
663 There are few experimental studies that report the solubility of Pd in silicate magma but they are
664 known to be much higher than Pt (Mungall and Brenan, 2014). A number of recent studies have
665 shown that direct crystallisation of PMM, particularly Pt-arsenide phases, can occur prior to
666 sulfide saturation (Helmy et al., 2013; Brenan et al., 2015; Helmy et al., 2015). There is almost
667 no As whatsoever in the Platinova Reef sulfides and the only semi metals present in any
668 consistently detectable amount in the laser ablation study of Holwell et al. (2015) were Te, Bi
669 (as minor PMM) and Se (in solid solution in sulfide). However, the PMM are primarily alloys of
670 Cu, or in our samples, also Pb. Therefore if separate saturation of PMM took place, it would
671 imply that the magma became saturated in Pd-Au-Cu and Pd-Pb alloys, that then acted as a
672 nucleation point for the Cu sulfides, and then saturated in Au-Cu alloy at a slightly later stage.
673
674 Whilst this is an attractive mechanism for producing the extremely high metal tenors and the
675 variable PMM-Cu sulfide ratios on a droplet scale, it would require the somewhat coincidental

saturation of the magma in PGM and sulfide liquids almost instantaneously, followed by saturation in AuCu (which has a liquidus of ~920°C; Okamoto et al. 1987), and whilst this does not preclude this mechanism, we view it as very unlikely. Furthermore, two immiscible melts in equilibrium with one another must be in equilibrium with the same solid phase. So if the silicate melt was saturated in Pd-Cu alloy, then the sulfide must have been too. The solubility of PdCu in Cu-Fe-S melt is in the order of tens of percent (Karup-Moller et al., 2013), and so the silicate melt cannot have been saturated with PdCu at the time the low tenor sulfide droplets formed. Therefore, we suggest that the sulfide droplets in the Pd-rich zones must have nucleated as Cu-Fe-S liquid with very high Pd contents, but not Pd-metal saturated.

9.2.2. Formation of extremely PM-enriched Cu-sulfide and subsequent modification

One major characteristic of the Platinova Reef sulfides is that the metal tenors are much higher than in any of the similar offset reef style deposits. One possible reason for this was proposed by Holwell and Keays (2014) and Nielsen et al. (2015) who advocate mechanisms by which the basal layer of magma from which the Platinova Reef formed was anomalously enriched in chalcophile elements. The proposed mechanisms differ somewhat, but essentially involve the addition of PM-enriched sulfides or silicate liquids derived from elsewhere in the chamber to a sulfide-undersaturated liquid layer at the floor, generating PGE enrichment in this liquid layer, which then becomes sulfide saturated to form high tenor sulfide microdroplets. Given some degree of Pd pre-enrichment, the high Pd tenors of some of the observed droplets could be explained in relation to the known extremely high partition coefficient for Pd (Mungall and Brenan, 2014). However, given the similar tenors for Au in the Au zone, this does not appear to be a possibility for Au (which has a much lower partition coefficient of ~1000); unless particular circumstances have led to anomalously high partition coefficients. That said, the positioning of a Au-rich zone above the PGE-rich zone is a consistent general feature of offset reef deposits, and as pointed out above the relative positioning of the Pd, Au and Cu peaks in Platinova is essentially identical to that in numerous other offset reefs with widely varying host cumulus mineralogy.

Assuming the formation of PM-enriched sulfide droplets, the observed variations in PMM-sulfide ratio could be formed if the droplets underwent subsequent modification. Possible mechanisms are: a) redissolution in a migrating sulfide-undersaturated or Fe-rich melt (Godel et al., 2014; Nielsen et al., 2015); b) incongruent destruction by oxidation (Wohlgemuth-Ueberwasser et al., 2012) selectively removing Fe-Ni-sulfide, or c) physical mechanicals driven by late stage

710 solidification and compaction such as separation of sulfide from solid PM phases during
711 percolation through the crystal mush, or preferential attachment to migrating vapour bubbles.
712 Essentially all these mechanisms alter the PM tenor by removing or decoupling sulfide and PM,
713 post-formation..
714
715 Godel et al. (2014) and Nielsen et al. (2015) interpret the higher Pd tenors in sulfides outside of
716 oxide grains to be a result of partial dissolution of sulfides not protected by entrapment in oxide.
717 If partial dissolution took place after the *in situ* growth and trapping of the sulfides, it would
718 require a change from sulfide saturated to undersaturated conditions. Nielsen et al. (2015)
719 attribute this dissolution to be caused by interaction with the immiscible Fe-rich liquids derived
720 from the intercumulus melt within their postulated crystal mush layer. The variability we observe
721 in silicate hosted blebs could be explained by the variable interaction with such a liquid.
722 However our samples are close to the margin of the intrusion and do not show evidence of
723 significant silicate liquid immiscibility in the form of the characteristic symplectites; and yet the
724 sulfide population is no different to that recorded from the more central parts (Godel et al., 2014;
725 Nielsen et al., 2015). Thus this mechanism does not fully explain the intrusion-wide features.
726
727 Wohlgemuth-Ueberwasser et al (2012) showed experimentally that the Cu/Fe ratio of sulfide
728 melt increases as a function of oxygen fugacity due to the preferential conversion of FeS into
729 FeO and $FeO_{1.5}$, and used this as an explanation for the low-volume Cu-rich sulfides in deposits
730 such as the Platinova Reef. However, we suggest that this is unlikely to be the case for the
731 Platinova Reef. Firstly, the oxidation model would require the Skaergaard magma to be highly
732 oxidised at the point of the Platinova Reef formation, which is unlikely given that magnetite had
733 been crystallising for some time. Secondly, and most convincingly, experimental work by Ripley
734 et al. (2002) showed that the first exsolution of sulfide liquid from strongly fractionated silicate
735 melt involves saturation in a Cu–Fe–S liquid phase, resulting in S-poor bornite solid-solution;
736 precisely the assemblage observed in the Platinova Reef. Thus an increase in Cu/Fe due to
737 oxidation of sulfide, while possible, is considered as unnecessary.
738
739 It is possible that sulfide liquid may have mechanically separated from the PMM, for example
740 due to necking and squeezing as the surrounding cumulates crystallised. This could produce a
741 population with variable PM tenors (as the nuggety PMM may be preferentially retained by one
742 portion of the split droplet). It could also explain the apparent consistency in Se tenor (Holwell et
743 al., 2015), that contrasts to the variability in PM tenor, as Se substitutes for S in the sulfide

portion and hence would not be fractionated by this process. However, if this was the case, one might expect to observe more clustered populations of sulfide blebs, which is not particularly obvious (Fig. 2, A1-3), although there is some evidence of squeezing along grain boundaries (Fig. 6E). Most importantly, the 3D textural relationships presented in Figure 11 show unambiguously that the sulfide liquid is very strongly wetting with respect to the PMM grains, making it very unlikely that these phases could be physically separated during postcumulus processes.

9.2.3. The effect of equilibrium and kinetic partitioning around growing sulfide droplets

The consistent sequence of PGE, Au and Cu peaks in offset reefs has been modelled in several examples by sequential fractional segregation of sulfide, and in all these cases the sequence can be predicted in terms of the relative values of the sulfide-silicate partition coefficient - highest for Pd, which is much higher than that for Au, which is slightly higher than Cu. Holwell et al. (2015) show a detailed series of peaks at the Au-Cu zone transition in the Platinova Reef of Au>Te>Se>Cu, upwards over a thickness of a few metres, entirely consistent with relative $D_{sul/sil}$ values. Thus, relative $D_{sul/sil}$ is likely to be the key control over the sequence of metal enrichment, though this does not in itself explain the high tenors.

Mungall (2002) states that at the point of nucleation, the effective R factor is extremely high, and thus the initial formation of sulfide droplets can produce very high tenors through kinetic effects. For an extreme example like the Platinova Reef, with exceedingly small sulfide droplets, the relative offsets may well be due to differences in $D_{sul/sil}$ value, but the tenors could also be explained by kinetic effects at the point of sulfide nucleation. Each droplet will initially be surrounded by a boundary layer depleted in those highly chalcophile elements that partition into the droplet. As such the very first, tiny droplets will be gain extremely high tenors immediately. However, this also has the effect of reducing the effective partition coefficient between the droplet and the far-field magma outside the boundary layer (or to decrease the effective R factor for each element). Mungall (2002) explains that the tenor variation at different stratigraphic heights is due to the interplay between the degree of supersaturation of the sulfide, which determines how fast the droplets grow, and the diffusivity of the PM species in question. Therefore, it is entirely possible that the extreme tenors in the smallest sulfides (in the Pd zone) are caused by these kinetic effects primarily, and the reduction in tenor with greater sulfide droplet size (Fig. 13) can be a result of sulfide growth.

9.3 Implications for the formation of offset reef deposits

The consistent sequence of metal offsets present in all offset reef deposits is compelling. On this basis, it is hard to believe that the Platinova system represents a fundamentally different set of processes than these other examples, and observed patterns are generally consistent with $D_{sul/sil}$ values at least in terms of their relative position. Kinetic effects on top of this are also likely to play a part. Mungall (2002) obtained a highly refined fit for the Munni Munni offset profile by including terms for diffusivity as well as for partition coefficients. The order of magnitude and order of peaks was essentially the same as that obtained by Barnes (1993) and Wilson and Tredoux (1990) for the Great Dyke using variation in partition coefficients only. A number of parallels from Mungall's (2002) modelling can be made with Platinova Reef, including the peaks in PGE being prior to the peak in Cu. Most interestingly, his modelling also shows a distinct peak in Au at the same point as where Cu increases: exactly where the main Au peak occurs in the Platinova Reef. The latter has much higher concentrations of Au, though this is likely in part to be a consequence of the more fractionated nature of the Skaergaard magma at the time of sulfide formation (also seen by the lack of any Ni or IPGE). As such, the primary control on the order of metal peaks in offset deposits appears to the relative $D_{sul/sil}$ value of the chalcophile element; although kinetic effects also play a role, in particular in allowing the very first droplets to become very high tenor at the point of nucleation. As sulfide segregation progresses, alongside fractionation, depletion of the magma in PGE (e.g. through the mechanism proposed by Latypov et al., 2013) will compound the reduction in tenor up through the sequence.

Our textural data supports an analogous physical mechanism of sulfide formation in the irrespective of the dominant PM (Pd or Au). We therefore favour models for the formation of the Platinova Reef and other offset reefs that allow for the formation of microdroplets of Cu sulfide that become enriched in precious and semi metals according to their relative $D_{sul/sil}$ value, but that may also be affected by diffusion of those cations, which is related to the time available for equilibratation, and the degree of sulfide supersaturation. Clearly, the change to higher sulfide volumes affects the ability for Au to partition into sulfide as this is a common feature of all such deposits, but this gives an *apparent* increase in its $D_{sul/sil}$ value. There may be some change in the speciation of Au in the melt which causes a big change in its *D* value (and perhaps diffusivity as well), with this happening at the same time as the degree of supersaturation in Cu(Fe)S liquid is changing at the point of the chamber-wide onset of sulfide saturation. Whatever the mechanism, this transition marks a fundamental change in partitioning behaviour, but not the physical mechanism of formation.

812

813 9.3.1. Implications for the formation of the Platinova Reef

814 This work implies a similar physical mechanism for PM-sulfide bleb formation, irrespective of the
815 dominant PM, and confirms the conclusions of previous studies that suggest *in situ* growth and
816 trapping of tiny PM-enriched cumulus sulfide droplets (Godel et al., 2014; Holwell and Keays,
817 2014; Nielsen et al., 2015). In addition to these aspects, our geochemical and mineralogical
818 data have a number of other implications that can be applied to models for the formation of the
819 Platinova Reef, including the role of magnetite, and hydrothermal activity.

820

821 The role of magnetite crystallisation in driving the Skaergaard magma to sulfide saturation has
822 been explored by a number of authors (Andersen, 2006; Holwell and Keays, 2014; Keays and
823 Tegner, 2015), with analogies made to other offset layers located in the upper parts of their host
824 intrusions, where the reefs are located where massive magnetite layers come in (Prendergast,
825 2000; Maier et al., 2003). Although there are no massive magnetite layers in the Triple Group,
826 the trigger for the Platinova Reef sulfides may still have been as a response to a more subtle
827 pulse of oxide crystallisation that pushed the magma to sulfide saturation. Tegner and Keays
828 (2015) show that cumulus sulfides in the Skaergaard Intrusion started to form at around 300 m
829 below the Platinova Reef, as a response to the first appearance of magnetite. These sulfides
830 formed at the crystal-magma interface, and it was not until the level of the Triple Group that
831 sulfide saturation took place in the whole-chamber. The fine resolution geochemical profiles
832 shown in Figure 5 show a significant peak in TiO_2 (a proxy for ilmenite) and V (magnetite) that
833 corresponds closely with the point where Pd starts to increase. This is a consistent feature of
834 the Platinova Reef sections studied by Prasser et al. (2015) and is also shown by Nielsen et al.
835 (2015). However, in detail, Pd actually starts to increase 40cm below the point where TiO_2 and
836 V increase. If magnetite did trigger the sulfide formation, this would imply a small scale
837 decoupling, and possible evidence of some minor downward percolation of sulfide droplets. Or it
838 could simply mean that the close association is the result of some other factor that could have
839 led to oxide and sulfide formation.

840

841 We emphasise that magnetite crystallisation is not critical to forming all offset reef-type deposits.
842 As noted above, Munni Munni and the Great Dyke both contain offset deposits in magnetite-free
843 cumulates that formed before onset of magnetite saturation. However the distinct correlation
844 shown here implies that magnetite crystallisation contributed to the culmination of factors that
845 triggered Platinova Reef formation (e.g. Keays and Tegner, 2015).

Andersen (2006) and Nielsen et al. (2015) have, to varying extents, advocated the role of syn or post-magmatic hydrous fluids transporting precious and other metals. Our data shows no systematic difference in the nature and intensity of alteration between the Au and Pd zones or between blebs of high and low sulfide to precious metal ratio; this precludes any significant late hydrothermal component to the PM concentration mechanism. However, there are a number of features that show hydrous melts or fluids were present during or after formation of the primary sulfides, such as the presence of hydrous silicates with sulfides and PMM that are trapped within Fe-Ti oxides (Fig. 4). Godel et al. (2014) interpreted these to be a product of the low-temperature equilibration of trapped silicate melt and trapped vapour or fluids by diffusive exchange with evolved trapped interstitial liquid during the late stages of solidification. Critically, the inclusions are not restricted to a particular zone, and thus not related to the different PM contents in different zones.

Rudashevsky et al. (2014; 2015) and Nielsen et al. (2015) suggest that the Au zone represents a late mineralisation event formed in already crystallised gabbro, caused by the migration of the volatile-bearing residual of Fe-rich immiscible silicate melt enriched in Au, with Au deposited on grain boundaries. We find no 3D textural evidence for any significant differences between the formation of the Au and Pd zone sulfides and associated PM, and very little evidence of Fe-rich silicate immiscibility in our samples. However, the Au mineralogy does show some evidence of low temperature formation. The most common Au-bearing mineral in the Au zone in our samples, and those from other drillholes in the vicinity (Nielsen et al. 2015), is the unnamed mineral Au_3Cu, whereas it is tetra-auricupride (AuCu) in the more central areas. Cabri et al. (2005) and Rudashevsky et al. (2004) also note the presence of this phase in their studies of the Platinova Reef. Outside the Skaergaard Intrusion, Au_3Cu is very rare, but in all other cases where it is found, it is thought to have a low-temperature hydrothermal origin (Verryn et al., 1991; Stumpfl and Clark, 1965; Knipe and Fleet, 1997). Okamoto et al. (1987) show experimentally that Au_3Cu is stable at temperatures below 240°C; consistent with its presence as a low temperature hydrothermal phase. At Skaergaard, its presence may indicate *in situ* recrystallisation at low temperatures, rather than fluid remobilisation of PMM. Alternatively, the Au_3Cu in the Platinova Reef may simply be a low temperature alloy formed during recrystallisation on cooling of the PM-sulfide blebs without mediation by hydrothermal fluid. Therefore whilst some alteration is present to varying degrees, we do not believe that fluid

activity mobilised precious metals, but may have produced some S-loss from some sulfides and recrystallized some PMM to low-temperature phases. More generally, we argue that a fluid-driven mechanism requires a wildly improbably coincidence in depositing Au at a precise and very specific stratigraphic level in textural associations identical to those in the Pd-rich zone; in all offset reef style deposits.

10. Conclusions

The relative position of the Pd, Au and Cu peaks in the Platinova package is essentially the same as that in numerous other examples of offset PGE reefs, notwithstanding many differences in finer detail. This is unlikely to be a coincidence and thus we suggest that the same overarching processes are responsible for the enrichment in metals, and relative offsets in peak metal concentrations in all offset reef deposits worldwide. The Platinova Reef is important in this respect as it is an extreme example of such a deposit which records the extreme enrichment of precious metals via equilibrium and diffusive partitioning into sulfide liquid microdroplets very close to their point of nucleation. Concentration of the majority of precious metals is by cumulus droplets of Cu sulfide nucleated and grown *in situ* at the interface between the magma and the crystal pile; and occurs prior to the appearance of more abundant and larger gravitationally settled sulfide droplets.. This feature is common in other offset reef deposits, and is marked by the major enrichment in Au. Although the metal ratios of PGE to Au in the Pd- and Au-rich offset zones differ, the textures and mineralogy show the physical mechanisms of concentration are the same in all zones indicating a similar physical method of concentration. The fundamental geochemical and kinetic controls on the sequence and extent of metal enrichment are their relative $D_{sul/sil}$ values and diffusivities. In the case of the Platinova Reef, the increase in Pd concentration is located at a major Ti-V peak suggestive of a link between magnetite crystallisation and the nucleation of tiny Cu-sulfide liquid droplets, although the existence of magnetite-free offset reefs in other intrusions implies that the role of magnetite is not universal. Thus, offset reefs can form in settings corresponding to the first onset of sulfide saturation in an evolving magma chamber, regardless of the precise mechanism that triggers attainment of sulfide liquid saturation, and record the process of sequential metal enrichment subsequent to the intial nucleation of sulfide droplets in the magma.

Acknowledgments

The samples used in this study are part of a collaborative project between Platina Resources Limited and the University of Leicester. Platina Resources Ltd, and in particular, Mark Dugmore

and Ben Sharp, are thanked for allowing access to this samples, and permission to publish these results. A component of this research was carried out on the X-ray fluorescence microscopy beam line at the Australian Synchrotron, Clayton, Victoria, Australia. We acknowledge financial support for this facility from the Science and Industry Endowment Fund (SIEF). We thank Martin de Jonge for his programming of complex scan control scripts, and David Paterson and Kathryn Spiers for beamline assistance during the experiment. Belinda Godel and Michael Verrall provided invaluable assistance with processing and collecting the microCT data, and Belinda Godel is thanked for reviewing a draft of this manuscript. We thank Troels Nielsen for exhaustive discussions of Skaergaard and Platinova geology. Jim Mungall and Rais Latypov are thanked for reviews that have improved the quality and clarity of the manuscript.

References

Andersen, J.C.Ø., 2006. Postmagmatic sulfur loss in the Skaergaard Intrusion: Implications for the formation of the Platinova Reef. Lithos 92, 198-221.

Andersen, J.C.Ø., Rasmussen, H., Nielsen, T.F.D., Ronsbo, J.C., 1998. The Triple Group and the Platinova gold and palladium reefs in the Skaergaard Intrusion: stratigraphic and petrographic relations. Economic Geology 93, 488-509.

Ballhaus, C., Sylvester, P.J., 2000. Noble metal enrichment processes in the Merensky Reef, Bushveld Complex. Journal of Petrology 41, 545–561.

Barnes, S.J., 1993. Partitioning of the platinum group elements and gold between silicate and sulphide magmas in the Munni Munni Complex, Western Australia. Geochimica et Cosmochimica Acta 57, 1277-1290.

Barnes, S.J., Hoatson, D.M., 1994. The Munni Munni Complex, Western Australia: stratigraphy, structure and petrogenesis. Journal of Petrol. 35, 715-751.

Barnes, S.J., Keays, R.R., Hoatson, D.M., 1992. Vertical and lateral compositional trends within the PGE-mineralized porphyritic websterite layer of the Munni Munni Complex, Western Australia. Australian Journal of Earth Sciences 39, 289-302.

Barnes, S.J., Fisher, L.A., Godel, B., Maier, W.D., Paterson, D., Howard, D.L., Ran, C.G., Laird, J.S., Pearce, M.A., 2016. Primary cumulus platinum minerals in the Monts de Cristal Complex, Gabon: magmatic microenvironments inferred from high-resolution x-ray fluorescence microscopy. Contributions to Mineralogy and Petrology, 171, 23.

Bird, D.K., Brooks, C.K., Gannicott, R.A., Turner, P.A., 1991. A gold-bearing horizon in the Skaergaard Intrusion, east Greenland. Economic Geology 86, 1083-1092.

Brenan, J.M., Canali, A.C., Sullivan, N.A., 2015. Solubility of the assemblage Pt-PtAs(melt) in basalt with implications for Pt-As complexing and As speciation. Goldschmidt Abstracts 2015, 383.

Brenan, J.M., Rose, L.A., 2002. Experimental constraints on the wetting of chromite by sulfide liquid. Canadian Mineralogist 40, 1113-1126.

Brooks, C.K., Nielsen, T.F.D., 1982. The E Greenland continental margin: a transition between oceanic and continental magmatism. Journal of the Geological Society of London 139, 265-275.

Cabri, L.J., Beattie, M., Rudashevsky, N.S., Rudashevsky, V.N., 2005. Process mineralogy of Au, Pd and Pt ores from the Skaergaard intrusion, Greenland, using new technology. Minerals Engineering 18, 887–897.

Campbell, I.H., Naldrett, A.J., 1979. The influence of silicate:sulfide ratios on the geochemistry of magmatic sulfides. Economic Geology 74, 1503–1506.

Chung, H.-Y., Mungall, J.E., 2009. Physical constraints on the migration of immiscible fluids through partially molten silicates, with special reference to magmatic sulfide ores. Earth and Planet Science Letters 286, 14-22.

Godel, B., 2013. High resolution X-ray computed tomography and its application to ore deposits: case studies from Ni–Cu–PGE deposits. Economic Geology 108, 2005–2019

Godel, B., 2015. Platinum-Group Element Deposits in Layered Intrusions: Recent Advances in the Understanding of the Ore Forming Processes, in: Charlier, B., Namur, O., Latypov, R., Tegner, C. (Eds.), Layered Intrusions. Springer, Heidelberg, pp. 379-432.

Godel, B., Rudashevsky, N.S., Nielsen, T.F.D., Barnes, S.J., Rudashevsky, V.N., 2014. New constraints on the origin of the Skaergaard intrusion Cu–Pd–Au mineralization: Insights from high-resolution X-ray computed tomography. Lithos 190-191, 27–36.

Helmy, H.M., Ballhaus, C., Fonseca, R.O.C., Wirth, R., Nagel, T., Tredoux, M., 2013. Noble metal nanoclusters and nanoparticles precede mineral formation in magmatic sulphide melts. Nature Communications DOI: 10.1038/ncomms3405

Helmy, H., Ballhaus, C., Fonseca, R., Bragagni, A., Heuser, A., 2015. Platinum-Group Elements Fractionation by Selective Complexing. Goldschmidt Abstracts 2015, 1226.

Holness, M.B., Nielsen, T.F.D., Tegner, C., 2007. Textural maturity of cumulates: a record of chamber filling, liquidus assemblage, cooling rate and large scale convection in mafic larered intrusions. Journal of Petrology 48, 141-157.

Holness, M.B., Stripp, G., Humphreys, M.C.S., Veksler, I.V., Nielsen, T.F.D., Tegner, C., 2011. Silicate liquid immiscibility within the crystal mush: late-stage magmatic microstructures in the Skaergaard intrusion, east Greenland. Journal of Petrology 52, 175-222.

Holwell, D.A., Keays, R.R., 2014. The formation of low volume, high tenor magmatic PGE-Au sulphide mineralisation in closed systems: evidence from precious and base metal geochemistry of the Platinova Reef, Skaergaard Intrusion, east Greenland. Economic Geology 109, 387-406.

Holwell, D.A., McDonald, I., Armitage, P.E.B., 2006, Platinum group mineral assemblages in the Platreef at the Sandsloot Mine, northern Bushveld Complex, South Africa. Mineral Magagazine 70, 83-101.

Holwell, D.A., Keays, R.R., McDonald, I., Williams, M.R. (2015). Extreme enrichment of Se, Te, PGE and Au in Cu-sulfide microdroplets: evidence from LA-ICP-MS analysis of sulfides in the

Skaergaard Intrusion, east Greenland. Contributions to Mineralogy and Petrology, 170 DOI:10.1007/s00410-015-1203-y

Irvine, T.N., Andersen, J.C.Ø., Brooks, C.K., 1998. Included blocks (and blocks within blocks) in the Skaergaard Intrusion: geological relations and the origins of rhythmic modally graded layers. Geological Society of America Bulletin 110, 1398-1447.

Karup-Møller, S., Makovicky, E., Barnes, S-J., 2008. The metal-rich portions of the phase system Cu-Fe-Pd-S at 1000°C, 900°C and 725°C: implications for mineralization in the Skaergaard intrusion. Mineral Magagazine 72, 947-951.

Keays, R.R., Tegner, C., 2015. Magma chamber processes in the formation of the low sulphide magmatic Au-PGE mineralization of the Platinova Reef in the Skaergaard Intrusion, east Greenland. Journal of Petrology

Kerr, A., Leitch, A.M., 2005. Self-destructive sulfide segregation systems and the formation of high-grade magmatic ore deposits. Economic Geology 100, 311-332

Kirkham, R., Dunn, P.A., Kucziewski, A., Siddons, D.P., Dodanwela, R., Moorhead, G., Ryan C.G., De Geronimo, G., Beuttenmuller, R., Pinelli, D., Pfeffer, M., Davey, P., Jensen, M., Paterson, D., de Jonge, M.D., Kusel, M., McKinlay, J., 2010. The Maia Spectroscopy Detector System: Engineering for Integrated Pulse Capture, Low-Latency Scanning and Real-Time Processing. AIP Conference Proceedings 1234, 240-243.

Knipe, S.W., Fleet, M.E., 1997. Gold-Copper Alloy Minerals from the Kerr Mine, Ontario: Journal of the Mineralogical Association of Canada 35, 573-586.

Latypov, R.M., O'Driscoll, B., Lavrenchuk, A. 2013. Towards a model for in situ origin of PGE reefs in layered intrusions: insights from chromitite seams of the Rum Eastern Intrusion, Scotland. Contrib Mineral Petrol 166, 309-327.

Latypov, R.M., Chistyakova, S. Yu, Page, A. Hornsey, R. 2015. Field evidence for the in situ crystallization of the Merensky Reef. J Petrol doi:10.1093/petrology /egv023.

1047 Li, C., Ripley, E.M., Oberthür, T., Miller Jr, J.D., Joslin, G.D., 2008. Textural, mineralogical and
1048 stable isotope studies of hydrothermal alteration in the main sulfide zone of the Great Dyke,
1049 Zimbabwe and the precious metals zone of the Sonju Lake Intrusion, Minnesota, USA.
1050 Mineralium Deposita 43, 97–110.
1051
1052 Maier, W.D., 2005. Platinum-group element (PGE) deposits and occurrences: Mineralization
1053 styles, genetic concepts, and exploration criteria. Journal of African Earth Sciences 41, 165–
1054 191.
1055
1056 Maier, W.D., Barnes, S-J., Gartz, V., Andrews, G., 2003. Pt-Pd reefs in magnetitites of the Stella
1057 layered intrusion, South Africa: A world of new exploration opportunities for platinum group
1058 elements. Geology 31, 885-888.
1059
1060 Maier, W.D., Rasmussen, B., Fletcher, I., Godel, B., Barnes, S.J., Fisher, L.A., Yang, S.H.,
1061 Huhma, H., Lahaye, Y., 2015. Petrogenesis of the ~2.77 Ga Monts de Cristal Complex, Gabon:
1062 evidence for direct precipitation of Pt- arsenides from basaltic magma. Journal of Petrology, doi:
1063 10.1093/petrology/egv035
1064
1065 Mavrogenes, J.A., O'Neill, H.S.C., 1999. The relative effects of pressure, temperature and
1066 oxygen fugacity on the solubility of sulfide in mafic magmas. Geochimica et Cosmochimica Acta
1067 63, 1173-1180.
1068
1069 McBirney, A.R., 1989. The Skaergaard Layered Series: I; Structure and average composition.
1070 Journal of Petrology 30, 363-397.
1071
1072 McDonald, A.M., Cabri, L.J., Rudashevsky, N.S., Stanley, C.J., Rudashevsky, V.N., Roass,
1073 K.C., 2009. Nielsenite, PdCu3, a new platinum-group intermetallic mineral species from the
1074 Skaergaard Intrusion, Greenland. Canadian Mineralogist 46, 709-716.
1075
1076 McKenzie, D., 2011. Compaction and crystallization in magma chambers; towards a model of
1077 the Skaergaard Intrusion. Journal of Petrology 52, 905-930.
1078

1079 Momme, P., Tegner, C., Brooks, C.K., Keays, R.R., 2002. The behaviour of platinum-group
1080 elements in basalts from the East Greenland rifted margin. Contributions to Mineralogy
1081 Petrology 143, 133-153.
1082
1083 Mungall, J.E., 2002. Kinetic controls on the partitioning of trace elements between silicate and
1084 sulfide liquids. Journal of Petrology 43, 749-768.
1085
1086 Mungall, J.E., Brenan, J.M., 2014. Partitioning of platinum-group elements and Au between
1087 sulfide liquid and basalt and the origins of mantle-crust fractionation of the chalcophile elements.
1088 Geochimica et Cosmochimica Acta 125, 265-289.
1089
1090 Naldrett, A.J., 2011. Fundamentals of Magmatic Sulfide Deposits. Reviews in Economic
1091 Geology 17, 1-50.
1092
1093 Namur, O., Humphreys, M.C.S., Holness, M.B., 2014. Crystallization of interstitial liquid and
1094 latent heat buffering in solidifying gabbros: Skaergaard intrusion, Greenland. Journal of
1095 Petrology 55, 1389-1427.
1096
1097 Nielsen, T.F.D., 2013. Origin of the world-class PGE-Au mineralisation in the Skaergaard
1098 intrusion by bulk S-saturation, accumulation, partial dissolution, and secondary reef formation.
1099 Geophysical Research Abstracts 15:EGU2013-7879.
1100
1101 Nielsen, T.F.D., Andersen, J.C.Ø., Brooks, C.K., 2005. The Platinova Reef of the Skaergaard
1102 Intrusion. In: Mungall, J.E. (ed) Exploration for platinum-group element deposits. Mineralogical
1103 Association of Canada, Short Course Series 35, 431-456.
1104
1105 Nielsen, T.F.D., Andersen, J.C.Ø., Holness, M.B., Keiding, J.K., Rudashevsky, N.S.,
1106 Rudashevsky, V.N., Salmonsen, L.P., Tegner, C., Veksler, I.V., 2015. The Skaergaard PGE and
1107 gold deposit: the result of in situ fractionation, sulphide saturation, and magma chamber-scale
1108 precious metal redistribution by immiscible Fe-rich melt. Journal of Petrology 56, 1643-1676.
1109
1110 Ohnenstetter, M., Johan, Z., Cocherie, A., Fouillac, A.M., Guerrot, C., Ohnenstetter, D.,
1111 Chaussidon, M., Rouer, O., Makovicky, E., Mackovicky, M., Rose-Hansen, J., Karup-Moller, S.,
1112 Vaughan, D.J., Turner, G., Pattrick, R.A.D., Gize, A.P., Lyon, I.C., McDonald, I., 1999. New

exploration methods for platinum and rhodium deposits poor in base metal sulphides – NEXTPRIM. Applied Earth Science (Transactions of the Institute of Mining and Metallurgy) 108, B119-150.

Okamoto, H., Chakrabarti, D.J., Laughlin, D.E., Massalki, T.B., 1987. The Au-Cu (gold-copper) system: Bulletin of Alloy Phase Diagrams 8, 454-474.

Paterson, D., de Jonge, M.D., Howard, D.L., Lewis, W., McKinlay, J., Starritt, A., Kusel, M., Ryan, C.G., Kirkham, R., Moorhead, G., Siddons, D.P., 2011. The X-ray Flurorescence Microscopy Beamline at the Australian Synchroton. AIP Conference Proceedings 1365, 219-222

Prasser, R.F., Holwell, D.A., Graham, S.D., 2015. Geochemical and mineralogical data across the Platinova Reef, Skaergaard Intrusion, and its implications for the genesis of discrete, offset, precious metal-enriched horizons. Applied Earth Science (Transactions of the IOM3) 124, 51-52.

Prendergast, M.D., 2000. Layering and Precious Metals Mineralization in the Rincón del Tigre Complex, Eastern Bolivia. Economic Geology 95, 113-130.

Ripley, E.M., Brophy, J.G., Li, C., 2002. Copper solubility in a basaltic melt and sulfide liquid/silicate melt partition coefficients of Cu and Fe. Geochimica et Cosmochimica Acta 66, 2791–2800.

Rudashevsky, N.S., McDonald, A.M., Cabri, L.J., Nielsen, T.F.D., Stanley, C.J., Kretser, Y.L., Rudashevsky, V.N., 2004. Skaergaardite, PdCu, a new platinum-group intermetallic mineral from the Skaergaard Intrusion, Greenland. Mineralogical Magazine 68, 615–632.

Rudashevsky, N.V., Rudashevsky, V.N., Nielsen, T.F.D., Shebanov, A.D., 2014. Au-Cu alloys and inter-metallides in Pd-Au ores of the Skaergaard massif. Proceedings of the Russian Mineralogical Society 143, 1-23.

Rudashevsky, N.V., Rudashevsky, V.N., Nielsen, T.F.D., 2015. Intermetallides and alloys of copper and palladium in ores of the Skaergaard massif. Proceedings of the Russian Mineralogical Society 144, 30-53.

Ryan, C.G., 2000. Quantitative Trace Element Imaging using PIXE and the Nuclear Microprobe. International Journal of Imaging System Technology 11, 219-230.

Ryan, C.G., Kirkham, R., Hough, R., Moorhead, G., Siddons, D., de Jonge, M., Paterson, D., De Geronimo, G., Howard, D., Cleverley, J., 2010a. Elemental X-ray imaging using the Maia detector array: The benefits and challenges of large solid-angle. Nuclear Instrument Methods A 619, 37-43.

Ryan, C.G., Siddons, D.P., Kirkham, R., Dunn, P.A., Kuczewski, A., Moorhead, G., De Geronimo, G., Paterson, D.J., de Jonge, M.D., Hough, R.M., Lintern, M.J., Hoard, D.L., Kappen, P., Cleverley, J., 2010b. The New Maia Detector System: Methods for High Definition Trace Element Imaging of Natural Material, in Denecke M A, Walker C T, eds. X-Ray Optics and Microanalysis, AIP Conference Proceedings 1221, 9-17.

Saunders, A.D., Fitton, J.G., Kerr, A.C., Norry, M.J., Kent, R.W., 1997. The North Atlantic Igneous Province. In: Mahoney, J.J., Coffin, M.F. (eds) Large Igneous Provinces: continental, oceanic and planetary flood volcanism. Geophysical Monograph 100, American Geophysical Union, Washington DC, 45-93.

Stumpfl, E.F., Clark, A.M., 1965. Electron-probe microanalysis of gold-platinoid concentrates from southeast Borneo. Transactions of the Institution of Mining and Metallurgy, 74, 933–946.

Tegner, C., Duncan, R.A., Bernstein, S., Brooks, C.K., Bird, D.K., Storey, M., 1998. 40Ar-39Ar geochronology of Tertiary mafic intrusions along the East Greenland rifted margin: Relation to flood basalts and the Iceland hotspot track. Earth and Planetary Science Letters 156, 75-88.

Tegner, C., Thy, P., Holness, M.B., Jakobsen, J.K., Lesher, C.E., 2009. Differentiation and compaction in the Skaergaard Intrusion. Journal of Petrology 50, 813-840.

Thy, P., Lesher, C.E., Tegner, C., 2009. The Skaergaard liquid line of descent revisited. Contributions to Mineralogy and Petrology 157, 735–747.

Tredoux, M., Lindsay, N.M., Davies, G., McDonald, I., 1995. The fractionation of platinum-group elements in magmatic systems, with the suggestion of a novel causal mechanism. South African Journal of Geology 98, 157-167.

Verryn, S.M.C., Merkle, R.K.W., von Gruenewaldt, G., 1991. Gold- and associated ore minerals of the Waaikraal Deposit, northwest of Brits, Bushveld Complex. European Journal of Mineralogy 3, 451-566.

Wager, L.R., Brown, G.M., 1968. Layered Igneous Rocks: Edinburgh and London, Oliver and Boyd, 588pp

Wilson, N.C., MacRae, C.M., 2005. An automated hybrid clustering technique applied to spectral data sets. Microscopy and Microanalysis 11,434-435.

Wilson, A.H, Tredoux, M., 1990. Lateral and vertical distribution of the platinum group elements, and petrogenetic controls on the sulphide mineralisation, in the P1 Pyroxenite layer of the Darwendale Subchamber of the Great Dyke, Zimbabwe. Economic Geology 85, 556-584.

Wohlgemuth-Ueberwasser, C., Fonseca, R., Ballhaus, C., Berndt, J., 2013. Sulfide.oxidation as a process for the formation of copper-rich magmatic sulfides. Mineralium Deposita 48, 115-127.

Wotzlaw, J-F., Bindemana, I.N., Schalteggera, U., Brooks, C.K., Naslund, H.R., 2012. High-resolution insights into episodes of crystallization, hydrothermal alteration and remelting in the Skaergaard intrusive complex. Earth and Planetary Science Letters 355–356, 199–212.

Figure captions

Fig 1 A: Location of the Skaergaard Intrusion in east Greenland. B: Generalised statigraphic column of the Skaergaard Intrusion. The Platinova Reef is located within the Triple Group, which makes up the upper 100m of the Middle Zone. C: schematic representation of the Triple Group and its mineralised layers. the relative location of PRL08-35A is shown as being close to the margins of the intrusion, thus only containing two main mineralised layers.

Fig 2 Chimage Tornado maps showing spatial distribution of modal mineralogy through samples from the A: Cu zone (306m), B: Au zone (319.4m) and C: Pd zone (327m). Sections are orientated with their long axis perpendicular to the modal layering, so the alignment of plagioclase is seen to run parallel to the model layering (N-S in the illustrated views).

Fig 3 Tornado XRF element maps showing the spatial distribution of sulfides (red), K-feldspar (green) and apatite (blue) in relation to plagioclase (black), pyroxenes (mid grey) and oxides (pale grey) represented by different Fe contents shown in shades of grey, for samples from the A: Cu zone (306m), C: Au zone (319.4m) and E: Pd zone (327m). Note that sulfide aggregates appear much larger than they actually are in this representation. Textural associations are summarised in the pie charts (B, D, F), which show the relative proportions of sulfide grain aggregates/blebs (by number of grains) in relation to silicate/oxide grain boundary type- e.g. 49% of sulfides in the Cu zone are located at grain boundaries between oxide minerals and any other phase. Pie charts refer to all samples analysed from the specified zone.

Fig 4 Backscattered SEM images of sulfide-silicate inclusions hosted by Fe-Ti oxides in . A: example of a rounded sulfide inclusion with hydrous silicates in ilmenite from the Pd zone (327 m); B: close up view of the inclusion in A, showing a Pd-Au-Cu alloy associated with hydrous silicates and bornite-digenite; C: example of a rounded sulfide-bearing hydrous silicate inclusion in ilmenite from the Au zone (319.8 m), with a grain of Au3Cu present within the sulfide. Also present is a silicate inclusion trail like those shown by Godel et al. (2014). some of these contain some sulfide. Abbreviations: ilm: ilmenite; cpx: clinopyroxene; pl: plagioclase; serp: serpentine; bi: biotite; bn-dg: bornite-digenite; mt: magnetite.

Fig 5 Downhole bulk rock geochemistry through the Platinova Reef in drill hole PRL08-35A. A: Cu, Pd and Au; B: TiO2, V and Pd; C: thin section scans from 319, 322, 325 and 328 m showing the difference in Fe-Ti oxide content within the gabbro. Data can be found in Table 2.

Fig 6 A: Summary of precious metal mineral types found through the subzone, Pd, Au and Cu zones of PRL0835A. See Table 1 for individual mineral compositions and data; B: example of a relatively large sulfide bleb, attached to an Fe-Ti oxide grain from the Cu zone. Very small PM minerals are also associated with the sulfide; C: example of Au3Cu and Pd telluride at the margin of a sulfide grain that is partially replaced by amphibole; D and E: examples of zvagintsevite associated with sub-rounded and altered sulfide from the Pd zone. Abbreviations: cpx: clinopyroxene; pl: plagioclase; ilm: ilmenite; amp: amphibole; bn-dg: bornite-digenite; el: electrum; pal: palarstenide; kot: kotulskite; zvy: zvyagintsevite

Fig 7 Synchrotron XRF element maps from the Pd zone. C and D show an area of one of the sections mapped, with Sr (red) highlighting plagioclase, Ti (green) highlighting ilmenite, and Fe (blue) highlighting magnetite (pale blue) and pyroxenes (dark blue). A, B, E and F show magnified areas containing Cu sulfide and PMM, with G and H showing further magnified areas of E and F, respectively. Each magnified section is shown with Au-Fe-Cu (left hand side) and Pt-Au-Cu (right hand side) as the RGB colour set. Abbreviations: plag = plagioclase, ilm = ilmenite, mt = magnetite, cpx = clinopyroxene, opx = orthopyroxene.

Fig 8 Synchrotron XRF element maps from the Au zone. D shows an area of the thin section mapped with Sr (red) highlighting plagioclase, Ti (green) highlighting ilmenite, and Fe (blue) highlighting magnetite (pale blue) and pyroxenes (dark blue). A-C and E-G show magnified areas containing Cu sulfide and PMM, with the Au bearing PMM picked out in red (Au), with the Cu sulfides shown in blue (Cu).

Fig 9 Summary of association data for sulfide belbs and precious metal minerals (PMM) from the synchrotron XRF mapping data shown in Table 3. A: sulfide associations in the Au zone; B: sulfide associations in the Pd zone; C: PMM associations in the Au zone; and D: PMM associations in the Pd zone.

Fig 10 Slices through HRXCT reconstruction of samples from the Pd (A-C), Au (D-F) and Cu (G-I) zones showing textural relationships of PMM, sulfides (sul), alteration amphiboles (amp) and

host clinopyroxene (cpx), plagioclase (pl), orthopyroxene (opx), ilmenite (ilm) and titanomagnetite (mt). See text for description of features. Full sequential slice movies through each sample are included in the electronic appendix.

Fig 11 3D isosurfaces showing the relationship between PMM (red) and sulfide (yellow) blebs from A-C: the Cu zone (306 m), showing very small PMM associated with relatively large sulfides; D-F: the Au zone showing a variety of PMM to sulfide ratios, and examples of rounded droplets (D and F) and altered and ragged morphologies (E); G-I: the Pd zone showing both rounded (G) and ragged, altered (H,I) sulfide morphologies. Note that there are multiple PMM associated with the sulfides. 3D visualisations of the images shown in B, E, and I can be found at, respectively:
https://data.csiro.au/dap/SupportingAttachment?collectionId=16932&fileId=1065
https://data.csiro.au/dap/SupportingAttachment?collectionId=16932&fileId=1066
https://data.csiro.au/dap/SupportingAttachment?collectionId=16932&fileId=1067

Fig 12 A, C, E: proportion by number of grains of small sulphide blebs with high PM/Cu ratios, large sulphide blebs with low PM/Cu ratios in Cu Zone and PGM with little or no sulphide in the Cu, Au and Pd zones; B, D, F) numbers of these blebs within plagioclase (plag), pyroxene (px) and oxides (ox) as well as at contacts of plagioclase and pyroxene grains and contact of oxides with other minerals in the Cu Zone.

Fig 13 A-C: PMM sizes as Equivalent Sphere Diameters (ESD) in the Cu, Au and Pd zones, respectively. D-F: Turkey box plots of D) the ratio of PMM/sulfide ratio, by ESD, showing an increase from Cu, through Au to Pd zones; (E) the ratio of PMM/sulfide ratio, by volume, showing an increase from Cu, through Au to Pd zones; (F) The volume of sulfides associated with the PMM, showing a clear increase in sulfide volume from the Pd, through Au, to Cu zone. Tukey Box Plots divide the ordered values of the data into four equal parts by finding the median and then the 25th and 75th percentiles (~ inter quartile range depending on duplicate values – IQR). The median is defined by a horizontal line within a box that spans the ~IQR and contains approximately 50% of the data. The mean is represented by a large black circle. The fence is defined here as the central box (IQR) extended by 1.5 times the length of the box towards the maximum and the minimum.

Figures in Supplementary Appendix:

Fig A2 Sequential slice movie through a 3 mm core of the Pd zone from 327 m, illustrating the 3D relationships of the sulfides and PMM. Note the small size of the sulfide. Darkest grey = plagioclase, mid greys = pyroxenes, pale grey = oxides (ilmenite appear smooth, magnetite has ilmenite exsolution lamellae, very light grey = Cu sulfides, white = PMM.

Fig A2 Sequential slice movie through a 3 mm core of the Au zone from 312.9 m, illustrating the 3D relationships of the sulfides and PMM. Note the slightly larger size of the sulfides compared to the Pd zone. Darkest grey = plagioclase, mid greys = pyroxenes, pale grey = oxides (ilmenite appear smooth, magnetite has ilmenite exsolution lamellae, very light grey = Cu sulfides, white = PMM

Fig A3 Sequential slice movie through a 3 mm core of the Cu zone from 306 m, illustrating the 3D relationships of the sulfides and PMM. Note the much larger size of the sulfides compared to the Pd and Au zones and the association of the sulfides to oxides. Darkest grey = plagioclase, mid greys = pyroxenes, pale grey = oxides (ilmenite appear smooth, magnetite has ilmenite exsolution lamellae, very light grey = Cu sulfides, white = PMM

1326 Table 1 Geochemical data for the main mineralised portion of PRL08-35A, as plotted in Figure

1327 5.

From (m)	To (m)	Zone	Au ppm	Pd ppb	Cu ppm	V ppm	Fe_2O_3 wt %	TiO_2 wt%
316.0	316.2	Cu	0.211	158	719	572	18.88	5.28
316.2	316.4	Cu	0.232	190	812	731	20.36	6.23
316.4	316.6	Cu	0.257	201	867	703	20.48	6.08
316.6	316.8	Cu	0.271	209	873	733	21.51	6.57
316.8	317.0	Cu	0.265	229	890	821	22.74	6.97
317.0	317.2	Cu	0.246	235	813	703	20.47	5.91
317.2	317.4	Cu	0.254	287	895	708	21.64	6.49
317.4	317.6	Cu	0.257	264	857	761	22.14	6.78
317.6	317.8	Cu	0.217	246	650	703	21.88	6.94
317.8	318.0	Cu	0.201	228	638	749	22.23	7.46
318.0	318.2	Cu	0.174	162	583	860	23.16	8.06
318.2	318.4	Cu	0.217	246	613	1213	26.84	10.41
318.4	318.6	Cu	0.173	253	540	988	24.92	9.42
318.6	318.8	Cu	0.123	201	477	703	21.9	7.95
318.8	319.0	Cu	0.160	170	462	808	23.7	8.98
319.0	319.2	Au	1.631	120	291	812	23.95	9.07
319.2	319.4	Au	3.753	115	346	821	23.93	8.48
319.4	319.6	Au	1.770	216	221	793	23.51	8.1
319.6	319.8	Au	0.819	269	192	809	23.22	7.57
319.8	320.0	Au	0.449	348	161	906	23.92	7.38
320.0	320.2	Au	0.346	399	168	691	20.98	5.87
320.2	320.4	Intermediate	0.339	421	164	652	20.46	5.27
320.4	320.6	Intermediate	0.303	498	225	570	18.91	4.73
320.6	320.8	Intermediate	0.281	492	164	625	20.55	5.14
320.8	321.0	Intermediate	0.328	555	176	596	20.03	4.87
321.0	321.2	Intermediate	0.273	532	193	598	20.09	4.65
321.2	321.4	Intermediate	0.283	655	178	595	19.95	4.59
321.4	321.6	Intermediate	0.292	568	157	665	20.86	5.05
321.6	321.8	Intermediate	0.323	544	140	711	21.31	5.19
321.8	322.0	Intermediate	0.301	474	175	686	21.18	5.1
322.0	322.2	Intermediate	0.234	393	174	616	20.03	4.55
322.2	322.4	Intermediate	0.116	271	169	686	21.42	5.03
322.4	322.6	Intermediate	0.120	246	220	652	21.47	4.95
322.6	322.8	Intermediate	0.077	244	134	841	23.03	5.74
322.8	323.0	Intermediate	0.076	252	137	851	23.49	5.79
323.0	323.2	Intermediate	0.106	278	136	668	20.16	4.47
323.2	323.4	Intermediate	0.100	306	139	952	23.89	5.89
323.4	323.6	Intermediate	0.098	352	154	1088	24.59	6.28
323.6	323.8	Intermediate	0.121	416	149	698	20.17	4.4
323.8	324.0	Intermediate	0.152	527	152	589	18.52	3.73
324.0	324.2	Intermediate	0.191	655	149	496	17.17	3.28
324.2	324.4	Intermediate	0.287	845	155	432	16.06	2.98
324.4	324.6	Pd	0.345	1118	180	426	15.71	3.13
324.6	324.8	Pd	0.414	1285	177	408	15.79	3.01

324.8	325.0	Pd	0.457	1578	182	418	16.21	3.24
325.0	325.2	Pd	0.563	1987	221	427	15.56	3.5
325.2	325.4	Pd	0.431	1909	152	493	17.39	3.84
325.4	325.6	Pd	0.510	2244	359	489	16.85	3.84
325.6	325.8	Pd	0.548	2505	177	498	17.22	4.08
325.8	326.0	Pd	0.518	2603	218	541	17.26	4.25
326.0	326.2	Pd	0.487	2921	233	568	17.03	4.56
326.2	326.4	Pd	0.466	2935	196	642	18.09	4.81
326.4	326.6	Pd	0.395	3068	216	613	16.56	4.82
326.6	326.8	Pd	0.298	3132	213	823	20.32	6.09
326.8	327.0	Pd	0.250	3084	214	857	20.83	6.68
327.0	327.2	Pd	0.216	3135	225	858	20.94	6.79
327.2	327.4	Pd	0.137	2634	188	777	18.83	6.4
327.4	327.6	Pd	0.080	2318	170	1102	22.27	7.83
327.6	327.8	Pd	0.082	2329	180	1311	26.04	9.05
327.8	328.0	Pd	0.062	2354	186	1223	24.18	8.47
328.0	328.2	Pd	0.071	2247	189	1066	23.63	7.97
328.2	328.4	Pd	0.059	1933	196	666	19.24	5.72
328.4	328.6	Pd	0.038	1580	211	758	20.28	6.13
328.6	328.8	Subzone	0.028	1244	166	854	21.8	6.87
328.8	329.0	Subzone	0.026	1198	166	1061	24.34	7.83
329.0	329.2	Subzone	0.029	1231	160	998	22.84	7.31
329.2	329.4	Subzone	0.030	1073	194	889	22.17	6.82
329.4	329.6	Subzone	0.025	1052	132	1021	23.81	7.34
329.6	329.8	Subzone	0.026	1067	160	923	22.43	6.95
329.8	330.0	Subzone	0.022	938	162	753	21.08	6.42
330.0	330.2	Subzone	0.022	948	182	719	20.79	6.4
330.2	330.4	Subzone	0.029	856	174	779	21.89	6.89
330.4	330.6	Subzone	0.022	885	154	753	21.41	6.69
330.6	330.8	Subzone	0.024	933	161	732	21.15	6.51
330.8	331.0	Subzone	0.024	1015	158	773	21.94	7.14

1328

1329 Table 2 Summary of precious metal minerals identified through the Platinova Reef in samples from drill hole PRL08-35A. Area is

1330 calculated by assuming an ellipse around the longest and perpendicular axes of each grain in section (Holwell et al. 2006).

			Cu zone		Au zone		Pd zone		Subzone		TOTAL	TOTAL
Mineral	Formula	Classification	n	area	n	area	n	area	n	area	n	area
Skaergaardite	PdCu	PM-Cu alloy					23	599			23	599
Zvyaginsevite	Pd3Pb	Pd Plumbide					14	240	2	539	16	779
Unnamed	Au3Cu	PM-Cu alloy			11	326					11	326
Vysotskite	PdS	PGE sulfide					7	112	1	91	8	203
Unconstrained	Pd-Te-As	PGE arsenide			2	45			5	630	7	675
Electrum	(Au,Ag)	Electrum	1	1	4	333			1	30	6	364
Vincentite	Pd3As	PGE arsenide			3	195	1	156			4	351
Tetra-aurocupride	AuCu	PM-Cu alloy	4	48							4	48
Atokite	Pd3Sn	Pd stannide					4	280			4	280
Braggite	(Pd,Pt)S	PGE sulfide					3	234			3	234
Palarstanide	Pd5(As,Sn)2	PGE arsenide	3	3							3	3
Keithconnite	Pd3Te	Pd telluride					1	80	1	35	2	115
Kotulskite	PdTe	Pd telluride			1	9			1	0	2	9
Cabriite	Pd2CuSn	Pd stannide	2	2							2	2
Unconstrained	Pt-Pd-As	PGE arsenide							1	0	1	0
Majakite	PdNiAs	PGE arsenide	1	2							1	2
Isomerteite	Pd11Sb2As2	PGE antimo-arsenide			1	120					1	120
Unnamed	Pd-Ge-Cu	Pd germanide					1	60			1	60
Unconstrained	Pt-Pd-Fe	PGE-Fe alloy					1	6			1	6

1331 Table 3 Summary of PGE mineral associations from the synchrotron XRF mapping.

1332 Abbreviations: ox = oxide, cpx = clinopyroxene, plag = plagioclase, PMM = precious metal

1333 mineral.

		Au zone Totals	%	Pd zone Totals	%
Total grain count of sulfide blebs		37		30	
Total grain count of PMM		55		140	
Sulfide association	Inclusion in oxide	1	2.7	0	
	Inclusion in clinopyroxene	9	24.3	8	26.7
	Inclusion in plagioclase	0		3	10.0
	Grain boundary: ox-ox	1	2.7	0	
	Grain boundary: ox-cpx	5	13.5	6	20.0
	Grain boundary: ox-plag	7	18.9	2	6.7
	Grain boundary: cpx-cpx	11	29.7	5	16.7
	Grain boundary: cpx-plag	3	8.1	5	16.7
	Grain boundary: plag-plag	0		1	3.3
PMM associations	Inclusion in sulfide	4	7.3	18	12.9
	Inclusion in oxide	1	1.8	4	2.9
	Inclusion in clinopyroxene	4	7.3	8	5.8
	Inclusion in plagioclase	0		7	5.0
	Grain boundary: sulfide	44	80.0	98	70.5
	Grain boundary: ox-cpx	1	1.8	4	2.9
	Grain boundary: cpx-plag	1	1.8	0	
PMM composition	Au-Cu	30	54.5	20	14.3
	Pd-Cu	0		52	37.1
	Pd other	0		28	20.0
	Au other	25	45.5	40	28.6
Sulfide alteration	<10%	13	35.1	4	13.8
	10-50%	17	45.9	11	37.9
	>50%	7	18.9	14	48.3

1334

1335

1336

Table in Supplementary Data

Table A1. Volume analysis of all sulfides and PMM grain identified in the 3D HRXCT analysis, as used in Figure 13.

1342 Fig1

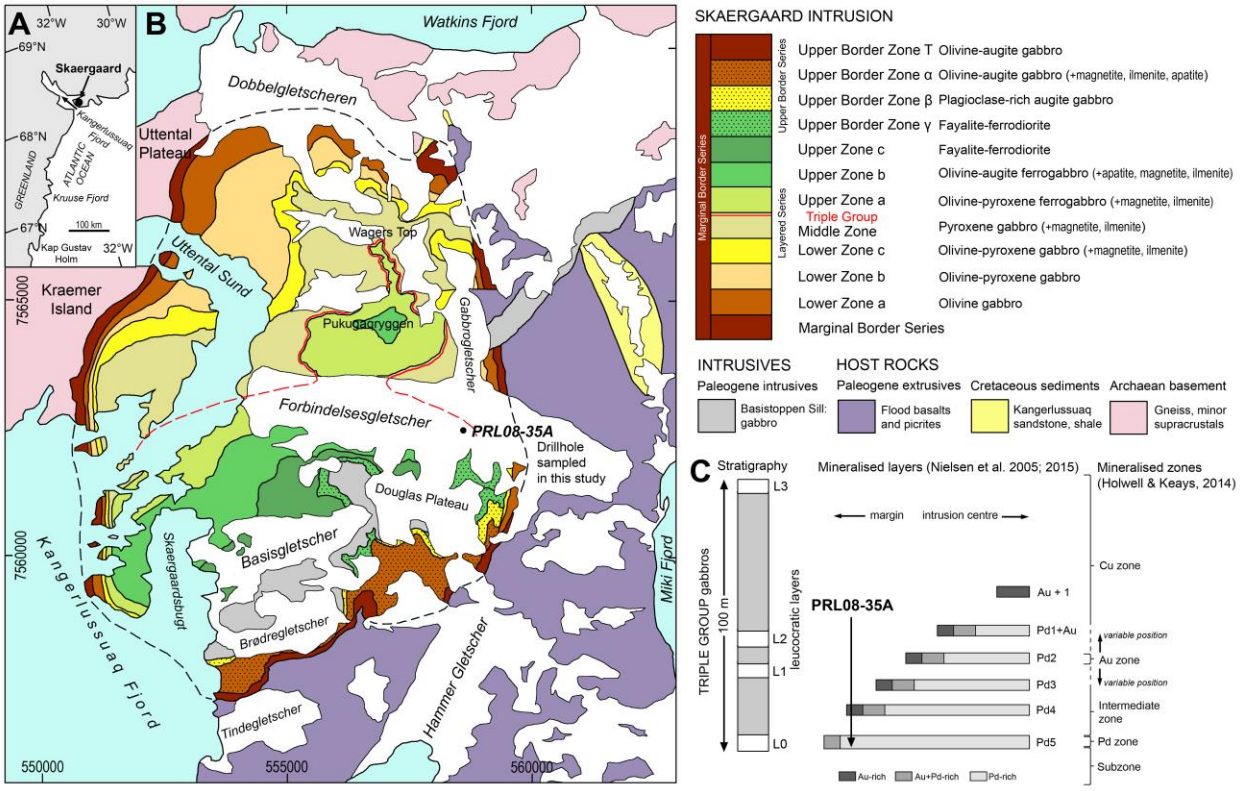

1343
1344

1345 Fig 2

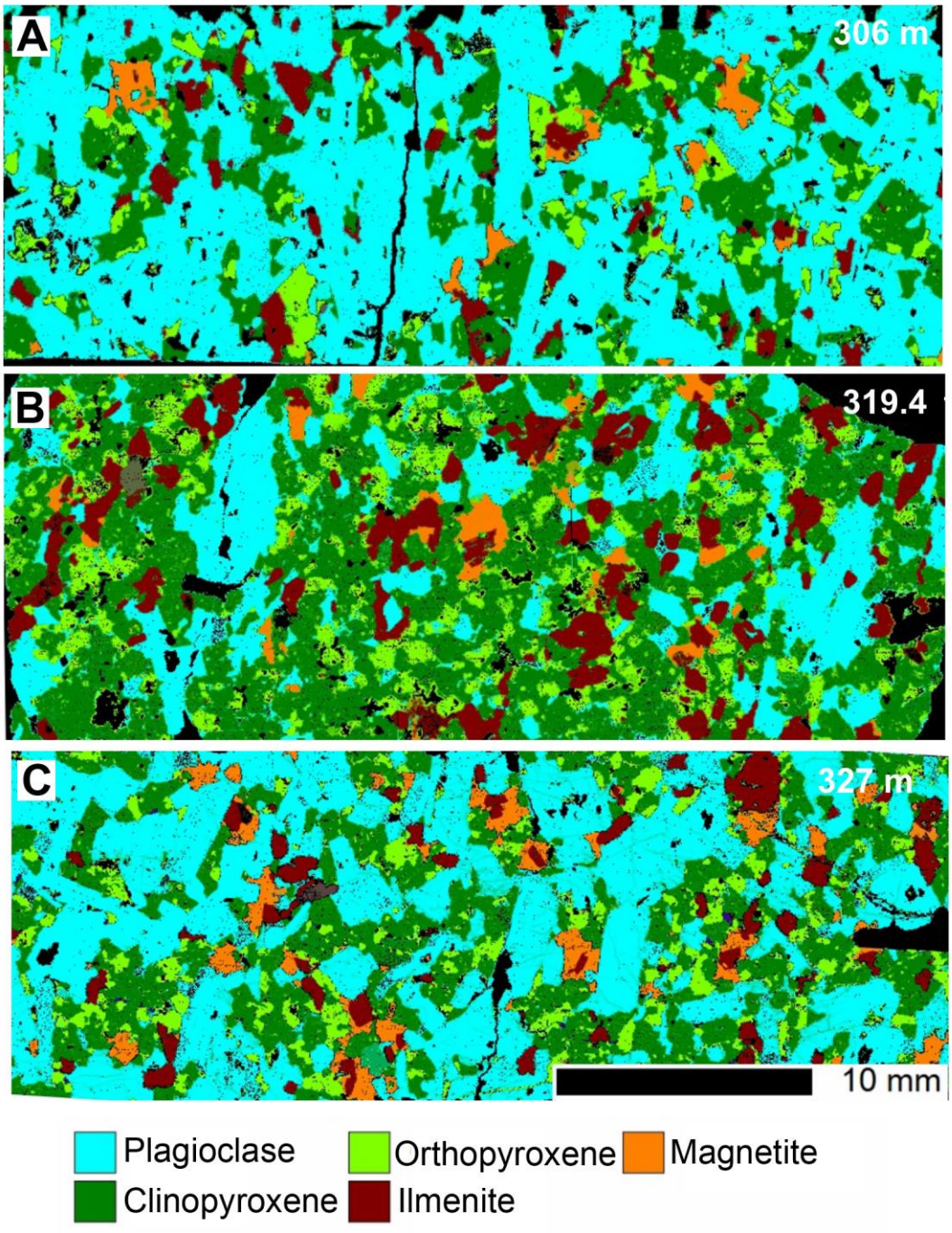

1346
1347

1348 Fig 3

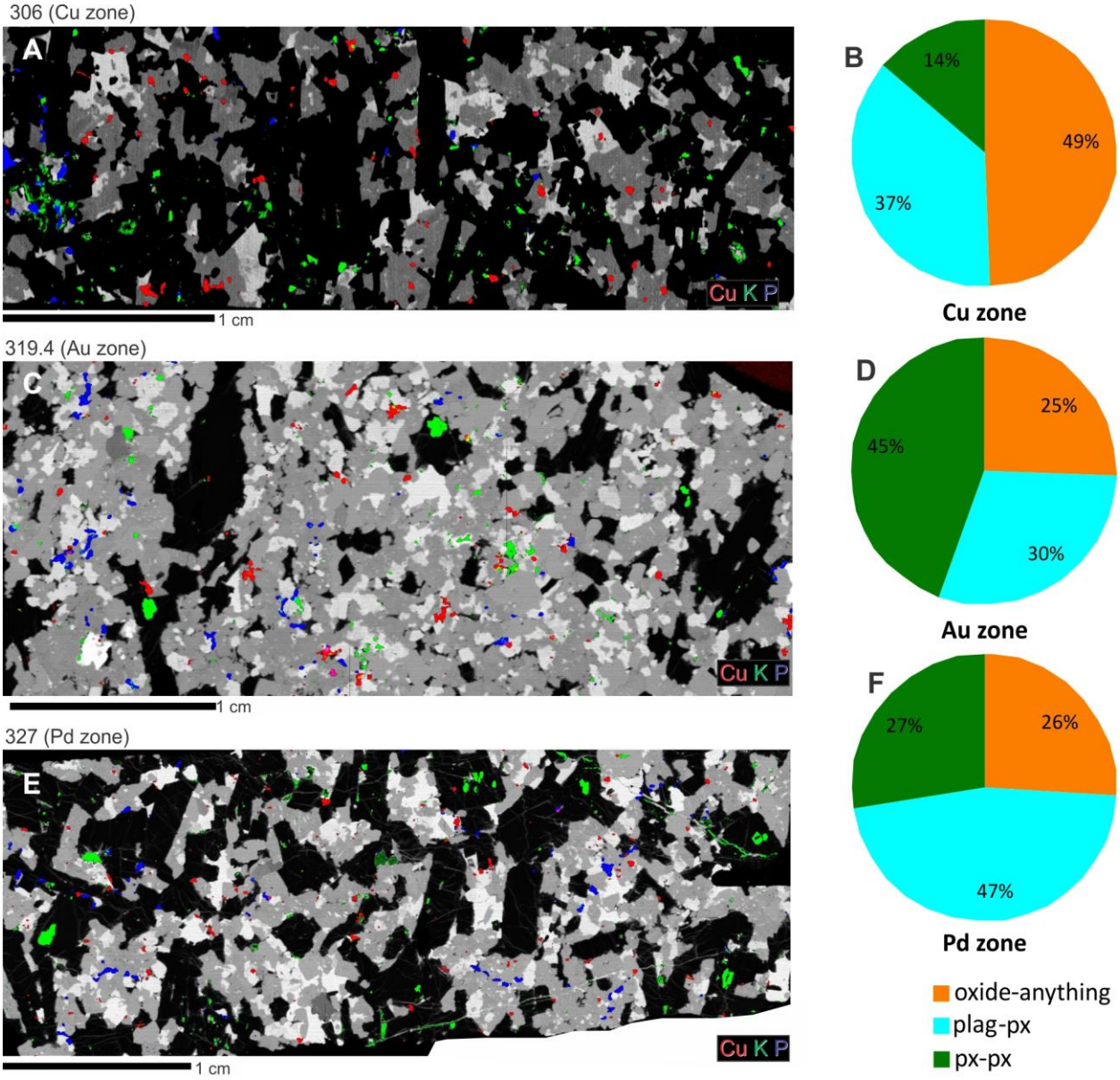

1349
1350

1351 Fig 4

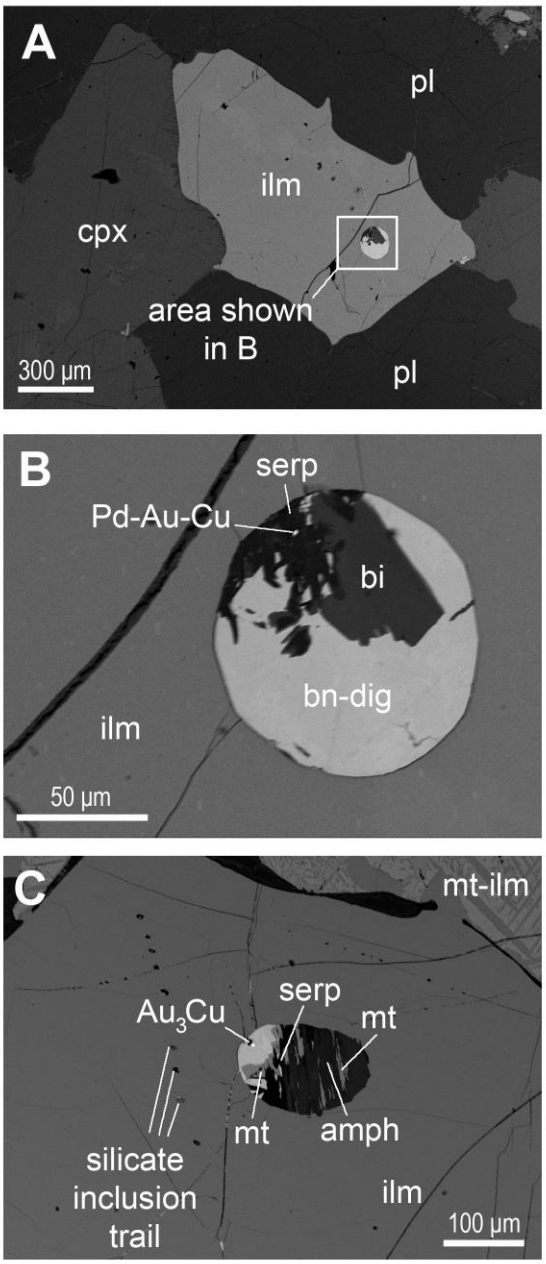

1352
1353

1354 Fig 5

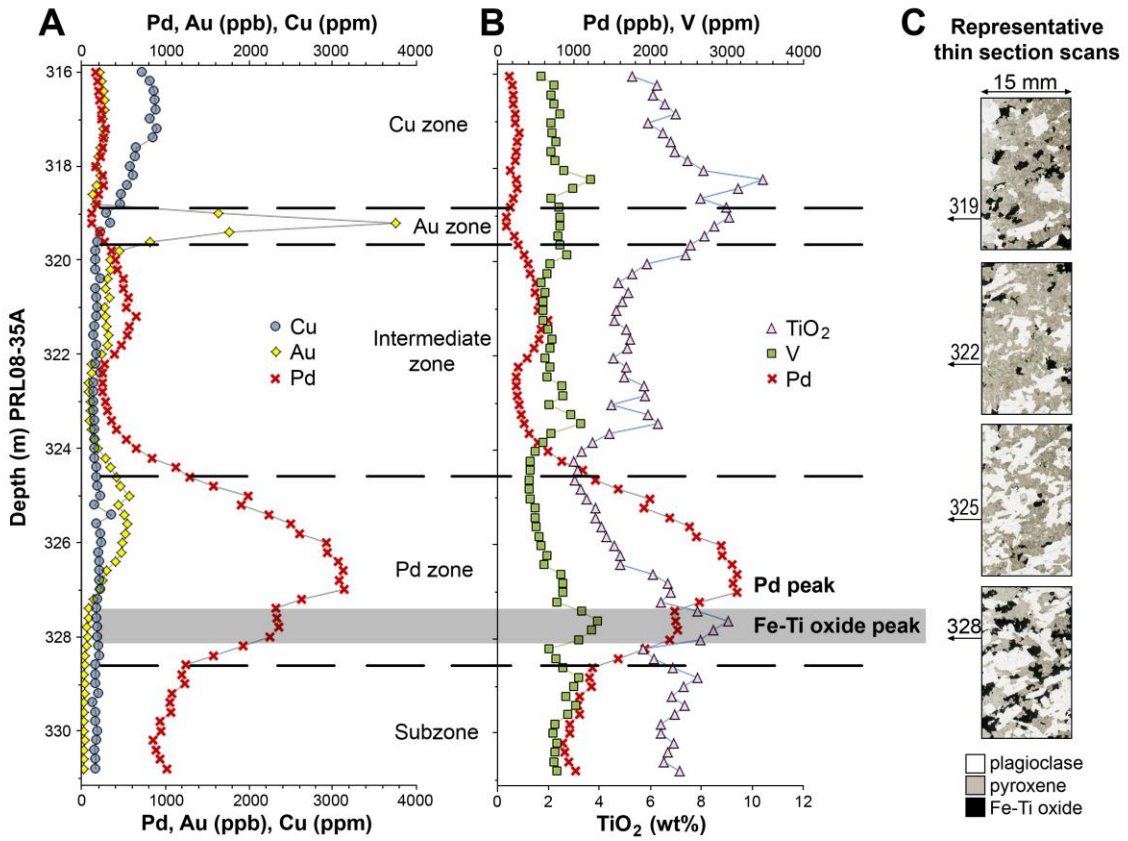

1355
1356

1357 Fig 6

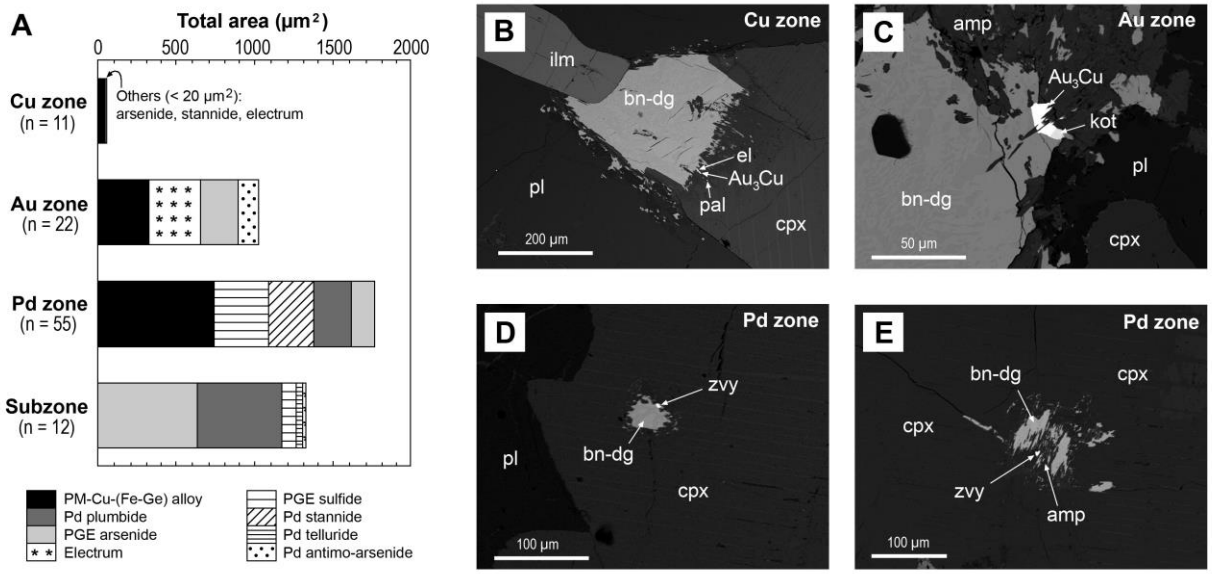

1358
1359

1360 Fig 7

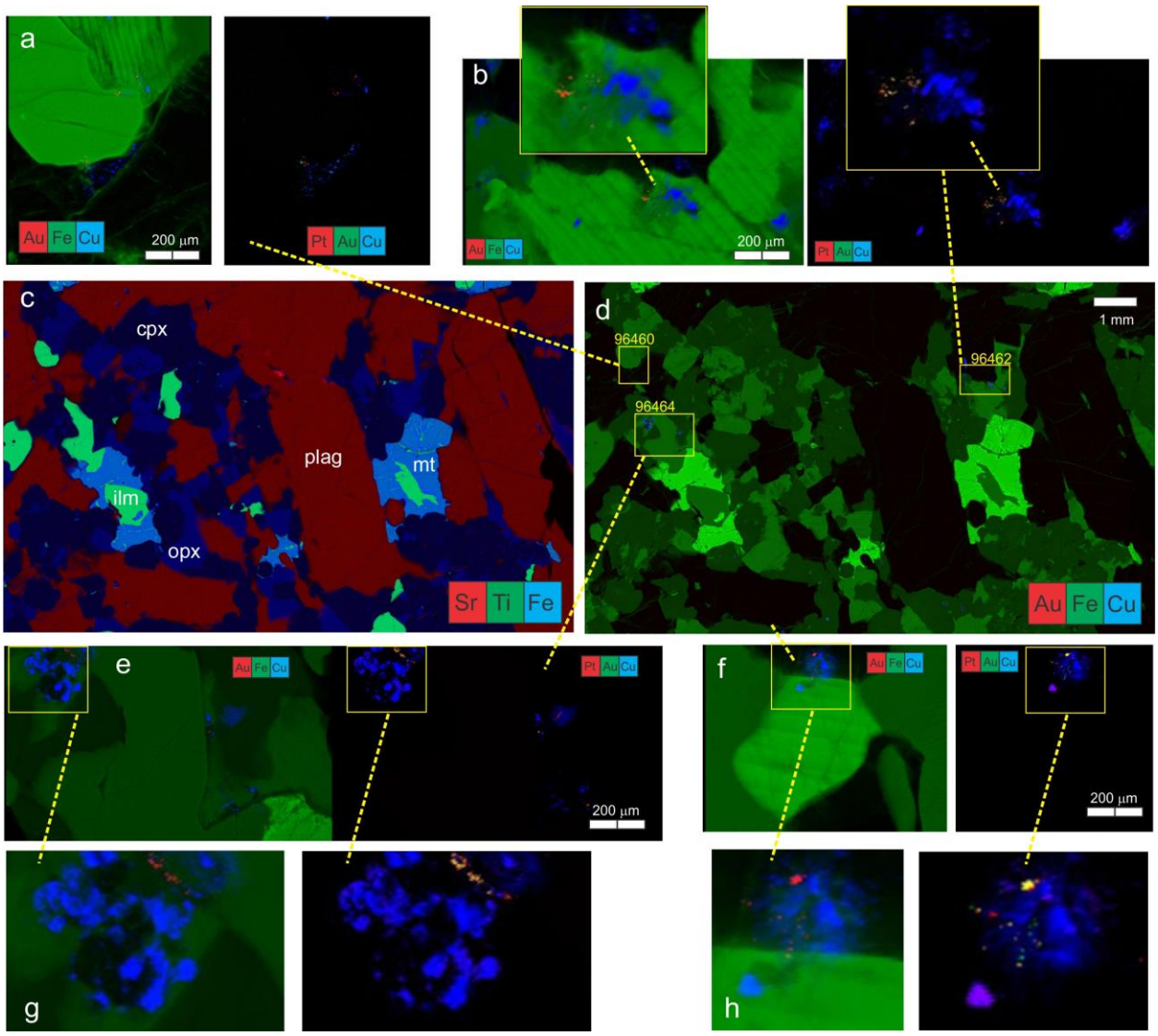

1361
1362

1363 Fig 8

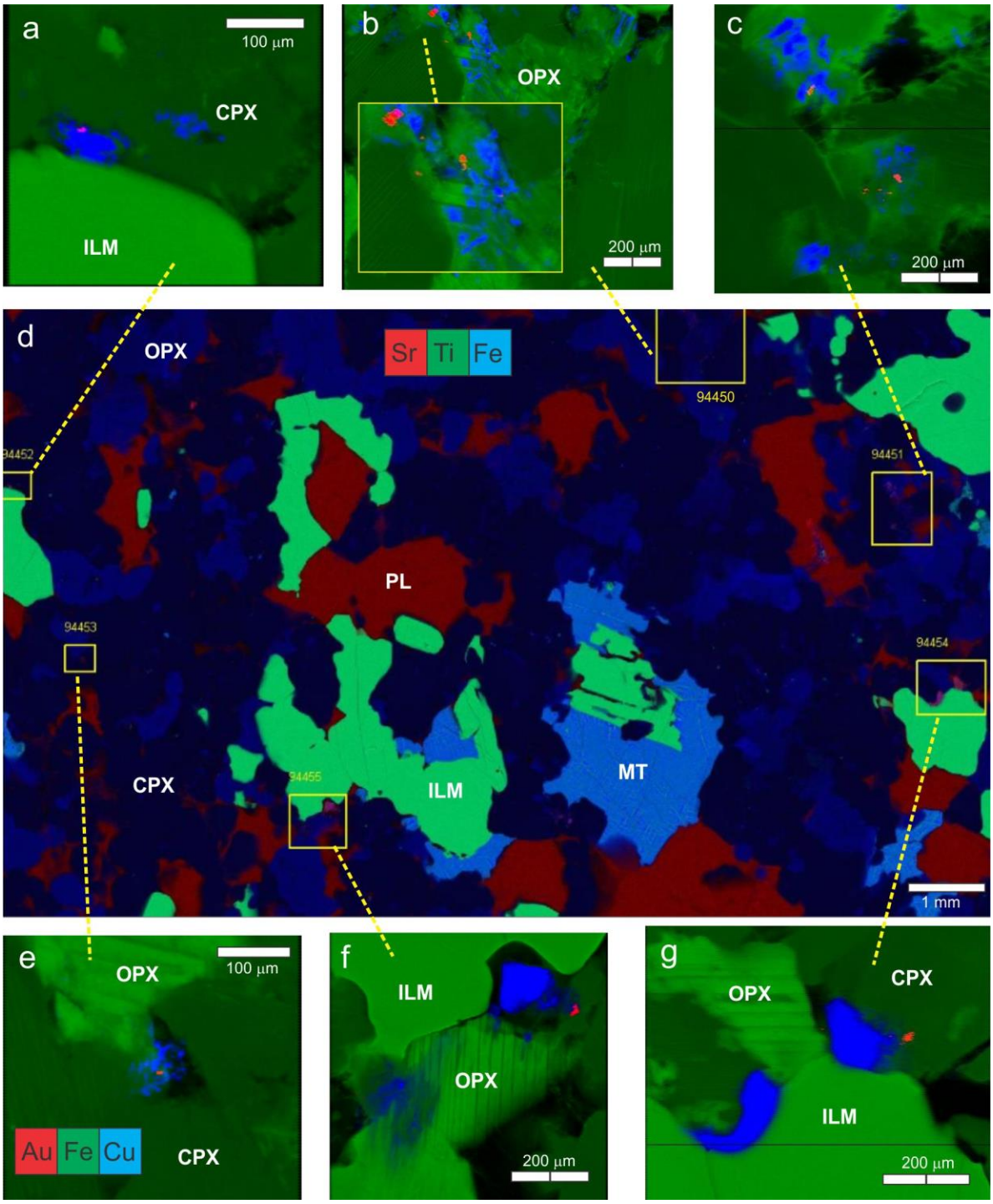

1364
1365

1366 Fig 9

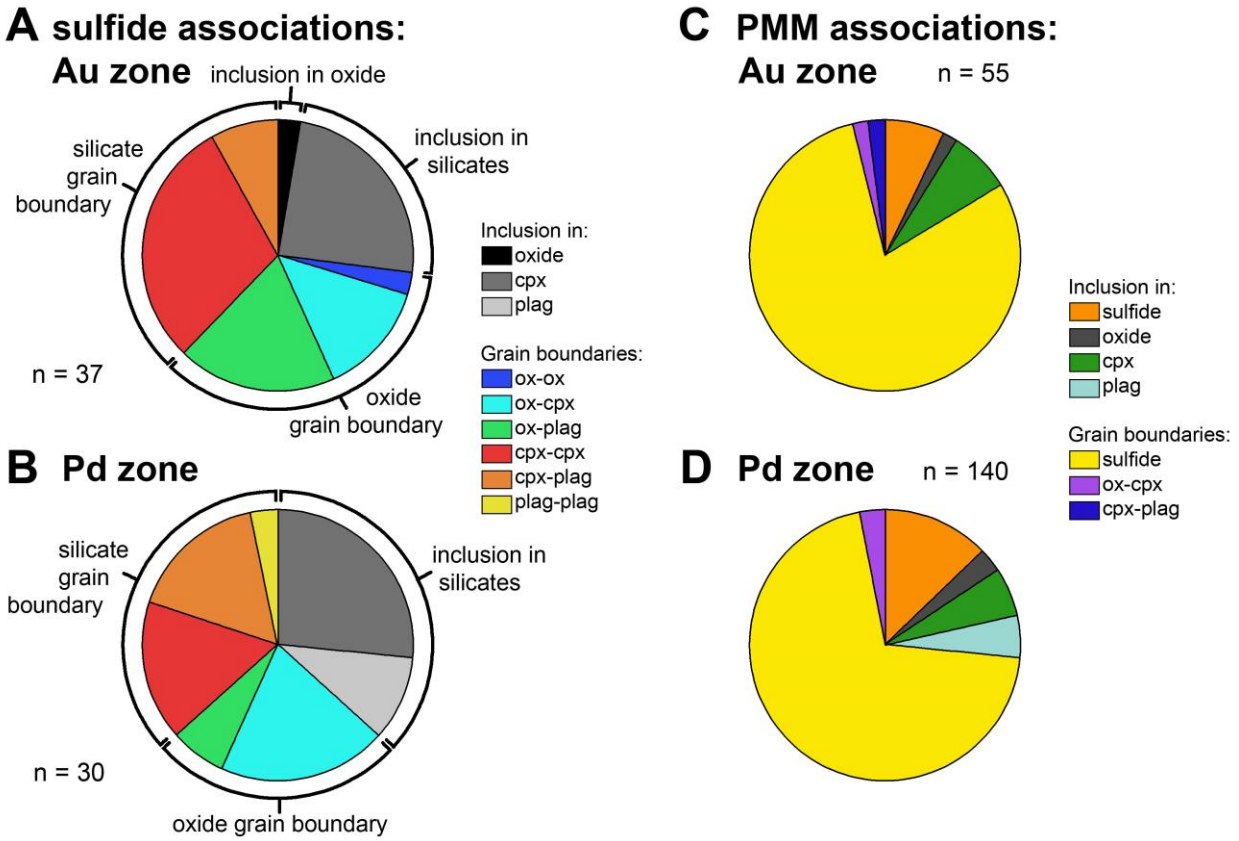

1367
1368

1369 Fig 10

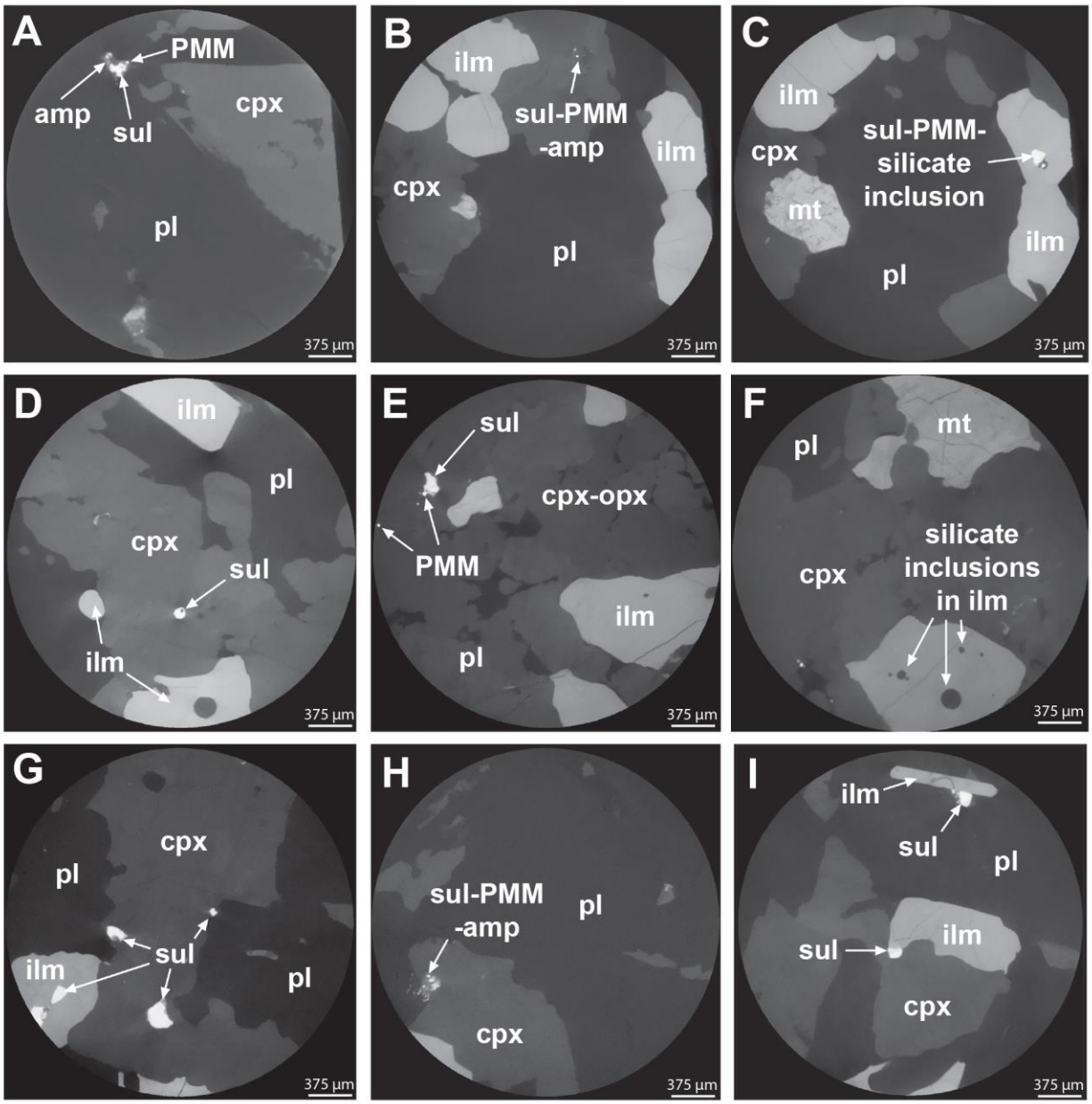

1370
1371

1372 Fig 11

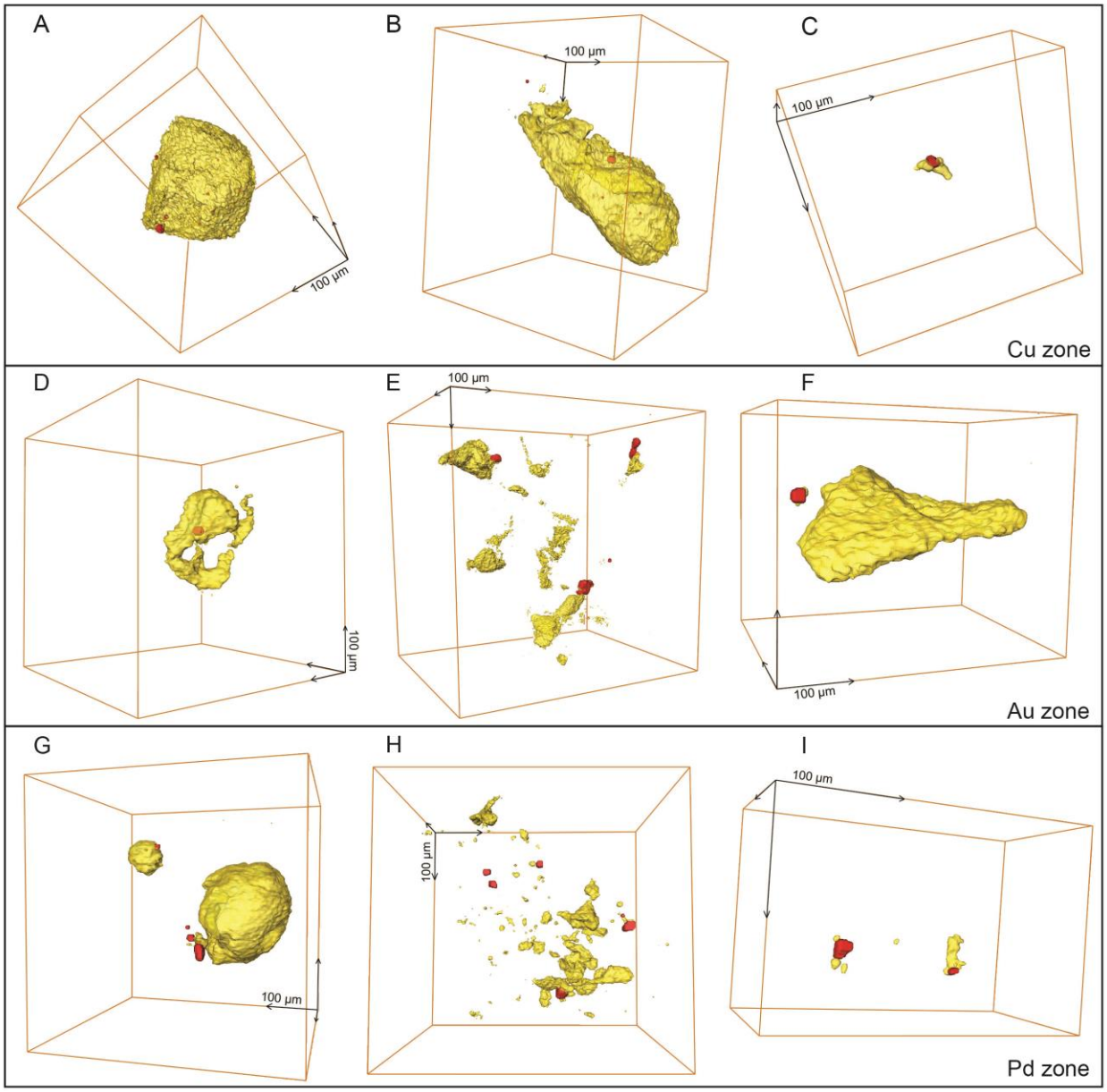

1373
1374

1375 Fig 12

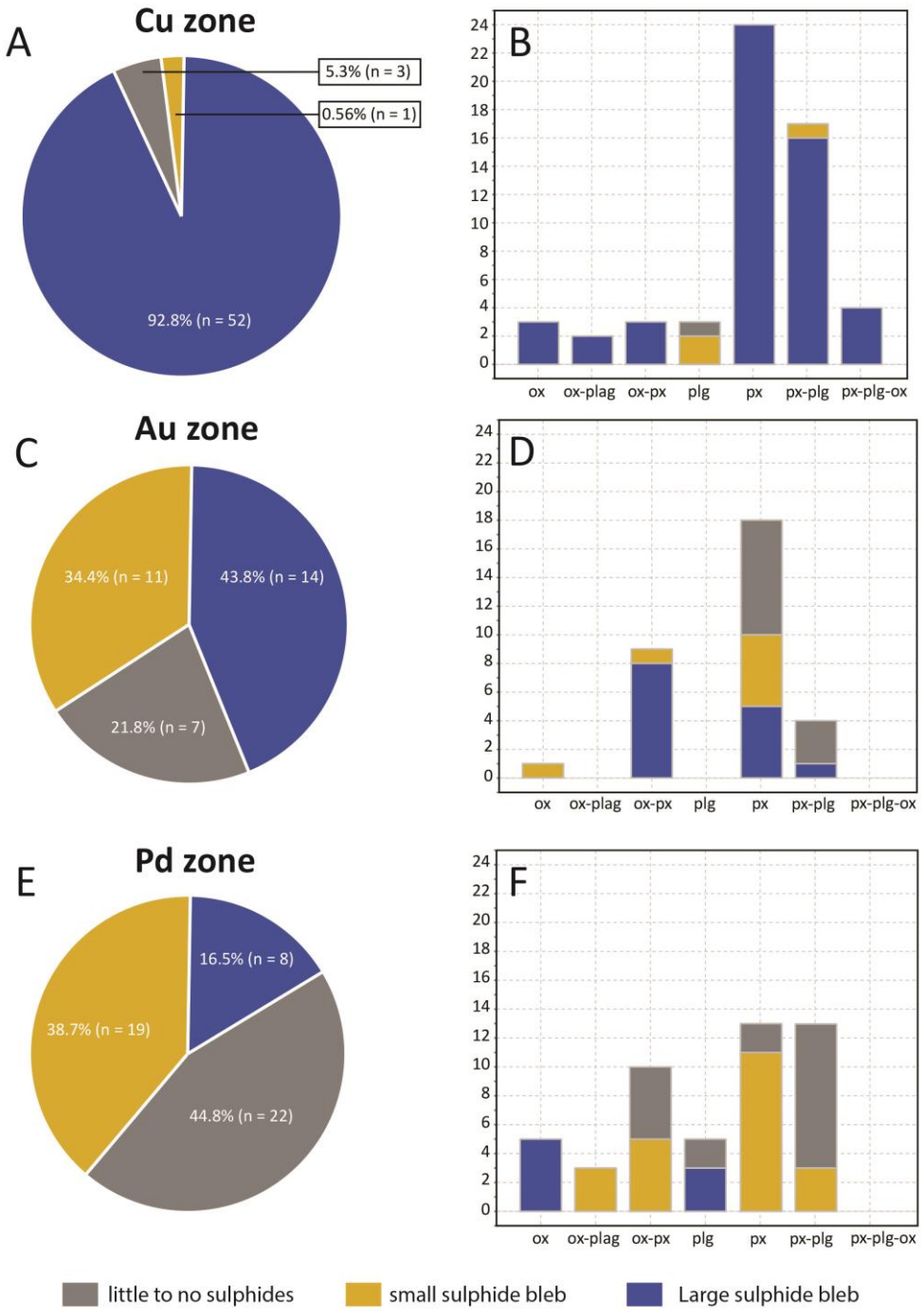

1376
1377

1378 Fig 13

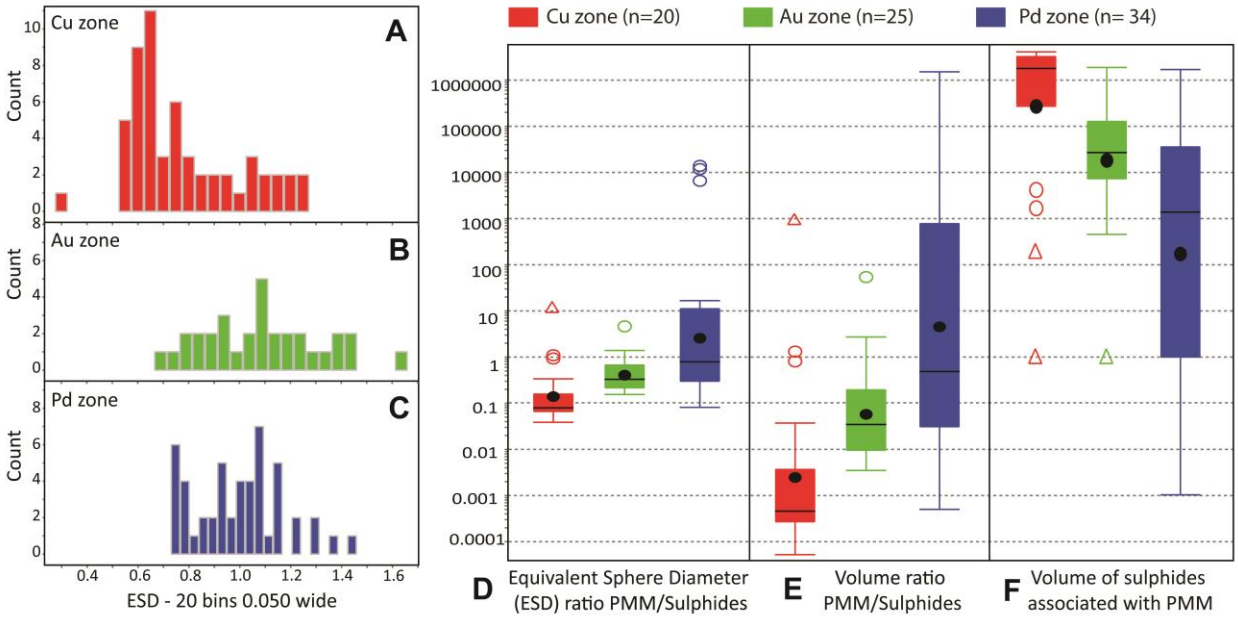

1379